Graphene wettability: fundamentals, modulations, and applications in energy fields

Yongfeng Huang[a,b,c*], Boyang Mao[d], Huanxin Li[e], Jincan Zhang[d*]

[a]*School of Material Science and Physics, China University of Mining and Technology, Xuzhou, Jiangsu 221116, China*
[b]*Songshan Lake Materials Laboratory, Dongguan, Guangdong 523808, China*
[c]*Beijing National Laboratory for Condensed Matter Physics and Institute of Physics, Chinese Academy of Sciences, Beijing 100190, China*
[d]*Department of Engineering, University of Cambridge, Cambridge, CB3 0FA, UK*
[e]*Department of Chemistry, Physical & Theoretical Chemistry Laboratory, University of Oxford, South Parks Road, Oxford OX1 3QZ, UK*

Abstract

Over the last decade, there has been a remarkable surge in the development of graphene-based energy generation, storage, transduction, and harvesting devices, driven by the exceptional electronic, optical, thermal, chemical, and mechanical properties of graphene. Notably, the tunable wettability of graphene offers an intriguing opportunity to enhance the performance of energy systems that utilize or involve water during device fabrication and usage stages, such as solar cells, nanogenerators, and supercapacitors. In this review, we provide an extensive overview of the latest research progress in the intrinsic wettability of graphene and its influencing factors, including substrate, contamination, defects, doping, and layer number. Subsequently, we highlight the representative applications in water-involved energy fields of high-quality graphene films synthesized via chemical vapor deposition. Lastly, we discuss current challenges in adopting graphene in the energy fields and propose future directions to promote the adoption of graphene in water-involved energy devices. Overall, this review presents critical insights into the significance of graphene wettability in advancing both the fundamental research and practical applications of graphene in energy fields.

Keywords: graphene; chemical vapor deposition; wettability; tunability; emerging energy devices

1. Background

The energy crisis is a global issue that has become increasingly urgent in recent decades due to population growth and climate change [1-4]. To tackle this challenge while protecting the environment, it is crucial to identify clean, sustainable, and accessible alternatives to fossil fuels [5, 6]. Among various renewable energy sources available, water is particularly promising due to its ability to absorb up to 35% solar energy reaching the Earth's surface and its prevalence in different forms, such as rivers, ocean waves, tides, raindrops, fogs, and dews [6-8]. Serving as a critical medium for energy storage, conversion, and transfer, water also facilitates the clean generation of electricity from heat or mechanical energy through various technologies such as hydro-voltaic technology [6, 8-10]. Moreover, most of the energy devices require the participation of water and the surface wettability of materials plays an important role. However, significant efforts are still required to enhance the performance of water-involved energy systems, such as energy transformation efficiency and stability.

Graphene has emerged as a promising platform for clean energy harvesting, storage, and transfer due to its unique structure and exceptional properties, such as high specific surface area, high electrical and thermal conductivity, high mechanical strength, chemical inertness, and tunable wettability [11-14]. Among the various methods for producing graphene materials, chemical vapor deposition (CVD) has shown great promise due to its fine controllability and scalability in synthesizing high-quality graphene film, particularly single-layer graphene (SLG) [15, 16], whose properties are comparable to those of its mechanical exfoliated counterpart and

* Corresponding author. Jincan Zhang; Yongfeng Huang Tel.: +44-07579913226.

E-mail address: jz543@cam.ac.uk; yfhuang@cumt.edu.cn

close to the theoretical predicted results [17-20]. Moreover, CVD graphene has already been adopted in diverse energy systems [21, 22], including solar cells [23, 24], batteries [25], supercapacitors [26, 27], nanogenerators [28, 29], heat transfer [30, 31], water harvesting [32], and defogging [33, 34], most of which requires the participation of water. Even though it is well-known that the water wetting states on graphene are highly related to the device performance [35, 36], the impact of the graphene wettability on water-involved energy devices has not yet been systematically summarized.

The wettability of graphene, which is determined by the interaction between water molecules and graphene, has long been a subject of debate, with conflicting reports on whether graphene is hydrophilic or hydrophobic [22, 37-40]. Experimentally, the measured water contact angle (WCA) of CVD graphene ranges from $< 30^{o}$ to $> 120^{o}$. This debate stems mainly from the high sensitivity of WCA measurement results to various factors, such as the structural imperfections of graphene, underlying substrates, and surface contaminations [22]. Recent studies employing large-area suspended CVD graphene and innovative wettability measurement techniques have provided conclusive experimental evidence of the intrinsic hydrophilicity in pristine graphene [41-43], therefore resolving this debate. What's more, recent research progress also provides clearer directions on how to tune the graphene wettability for different scenarios in energy fields [21]. Therefore, a review providing clear and systematic information on the relationship between CVD graphene structures and its wettability, as well as the strategies for wettability regulation, will be beneficial to facilitate the application of graphene in energy fields.

This review aims to provide a comprehensive overview of graphene wettability and its applications in CVD graphene-based water-involved energy systems (Figure 1), thereby contributing to the rapid development of clean and renewable energy. We begin by presenting the recent research progress on the graphene wettability by covering both the theoretical simulations and experimental results and then outline the key factors that influence the graphene wettability, including external factors (substrate and contamination) and internal structural factors (e.g., defect, grain boundary, wrinkle, layer number and doping). A variety of methods used to tune graphene wettability are also summarized. Next, we discuss the impacts of graphene wettability on solar cells, batteries, supercapacitors, nanogenerators performance, and the heat transfer, and water harvesting processes systematically. Finally, we provide a summary and perspective on the future direction of research in this area.

2. The intrinsic wettability of pristine graphene

This section aims to provide a clear understanding of the wettability of pristine graphene, by outlining the main theory, methodology, and external influence factors. Both the past controversies surrounding this topic and updated conclusion drawn from recent research will be covered.

2.1. Interactions between water molecules and graphene

The wettability of graphene is determined by the interactions between water molecules and graphene, which can be quantitatively represented by the adsorption energy or binding energy of water monomer on the graphene surface [39]. A clear relationship between the wetting state and the adsorption energy of water molecules on the graphitic surface has been reported, implying that higher adsorption energy, smaller WCA [44]. First-principles simulations based on the density functional theory are commonly used to calculate the adsorption energy of water molecules on graphene for which the one-leg and two-leg configurations are most constructed (Figure 2a) [45, 46]. Molecular dynamics (MD) simulations are conducted using empirical parameters derived from fitting the adsorption energy as a function of the distance from the oxygen atom in water to the graphene to obtain the intuitive wetting state of water droplets on the graphene [47]. The contact angle (CA) of water

droplets on graphene sheets, is then determined by fitting its profile (Figure 2b, c) [48].

The adsorption energy of water molecules on graphene is composed of dispersion [van der Waals (vdW)] and polarization (hydrogen bonding) forces. In 2012, Ikutaro Hamada considered the water-graphene interaction by means of the vdW density functional (vdW-DF) [49] and derived the adsorption energy > 75 meV at a distance of ~ 0.34 nm. He also pointed out that graphene is polarized, and the electrostatic interaction contributes to the adsorption energy [49]. Enge Wang *et al.* found that the adsorption energy of water monomer on graphene is > 70 meV at an almost same distance (0.34 nm), whose quantitative value is highly dependent on the functional [46]. In 2017, Daniel Blankschtein *et al.* emphasized the role of many-body polarization on the wettability of the graphitic surface, arguing that the polarization force has a more pronounced effect than the dispersive interaction on the interfacial entropy of water, which affects the graphene wettability [50]. They first calculated the binding energy of water monomer on the graphene-like polycyclic aromatic hydrocarbons using the symmetry-adapted perturbation theory and then fitted the adsorption energy *vs.* distance by Lennard-Jones equation to obtain empirical parameters for MD simulations. Their MD simulations showed that WCA on graphene is ~ 40°, indicating that the graphene is hydrophilic.

The hydrophilicity of pristine graphene is associated with the H-π interactions between water molecules and graphene. Zhongfan Liu *et al.* reported a fitted WCA of ~ 30° for water droplets on pristine graphene based on MD simulations (Figure 2d) [41]. They conducted accurate first-principles simulations to investigate the water-graphene interactions (Figure 2e) and acquired an adsorption energy of ~ 117.5 meV using the one-leg configuration. The charge distribution analysis showed that the intrinsic hydrophilicity of graphene is owing to the formation of H-π interactions. Electron transfers from the π bands of graphene towards H atoms in the water molecule is clearly observed (Figure 2f) and the water molecule would impact the charge distribution of graphene in regions larger than 2 nm (Figure 2g). The planar-averaged electron density as a function of water height further presents that the total amount of charges transferred from graphene to water along the z direction is 0.0221 electron (Figure 2h). Similar results have also been acquired for the two-leg configuration, further confirming the hydrophilicity in the pristine graphene.

2.2. Wetting transparency of graphene

The wetting transparency of graphene has been the subject of research for over a decade using both theoretical calculations and experimental methods (Figure 3a, b). However, the conclusions drawn from these studies are often contentious, and heavily dependent on the specific investigation scenarios.

To investigate the wetting transparency of graphene, attentions have been mainly focused on the features of substrates at the beginning; subsequently, various substrates and probe liquids have been adopted for clear comparisons and to figure out the contributions of polar and dispersive interactions [42, 45, 51]. Nikhil A. Koratkar *et al.* first investigated the wetting transparency of graphene using the large-area CVD graphene (Figure 3c). They clarified that when the vdW force dominates wettability of the substrates, such as Cu, Au and Si, graphene is wetting transparent. In contrast, when the short-range chemical bonding dominates the wettability for the substrates, such as glass, graphene is not wetting transparent anymore [52]. Daniel Blankschtein *et al.* revealed that the wetting transparency breaks down significantly on superhydrophobic and superhydrophilic substrates (Figure 3d) [53], implying that graphene is partially wetting transparent. Recent works elucidate the influences of substrates on the wettability of graphene and ends the dispute on the wetting transparency of graphene to a certain extent by calculating both the polar and dispersive components of the surface energy [54]. Grégory F. Schneider *et al.* measured the WCA of graphene on different substrates to cover a range of polarity and quantified the transparency of graphene towards polar and dispersive interactions, demonstrating the hydrophilicity of graphene (Figure 3e, f). Jianxiang Wang *et al.* used polar water, non-polar diiodomethane, and glycerol as probe liquids and demonstrated that graphene screens the polar surface energy

of the substrates (e.g., glass) but increases the dispersive surface energy [55]. The polar transmittance of graphene on SiO_2, Al_2O_3, oxidized polydimethylsiloxane (PDMS), Si and glass was also calculated, with an average value of 18.3% (Figure 3g). The authors concluded that the wetting transparency of graphene depends on how the reduced surface energy is compensated by the insertion of graphene. At the same time, the wetting transparency of graphene decreases significantly with the increase of layer number (Figure 3a, b). However, the reported number of graphene layers for which the wetting transparency completely vanishes ranges from 2 to 10, which highly relies on the substrate type.

When graphene covers substrates with a flat surface, the wetting behaviors are easy to understand, as discussed above. However, for rough surfaces, three wetting modes, including penetrate, Wenzel, and Cassie Baxter modes, need to be considered to determine the equilibrium and metastable contact states [56]. Lianfeng Sun *et al.* transferred the CVD few-layer graphene (FLG) onto flat and holey SiO_2 substrates and obtained WCAs of 83° and 93° respectively [57]. In their work, graphene almost completely complies with the morphology of the holey substrate with micron-scale holey array, which contributes to the change from hydrophilicity to hydrophobicity. Antonio Checco *et al.* varied the area fraction of suspended graphene from 0 to 95% by means of nanotextured substrates and concluded that completely suspended graphene exhibits the highest WCA (85° ± 5°) in comparison with the partially suspended or supported graphene, regardless of the substrate wettability [58]. They also reported that SLG could screen 80% long-range water-substrate interactions and the primary determining factor for the wettability of graphene is the short-range graphene-liquid interactions. Furthermore, Luquan Ren *et al.* fabricated hydrophobic graphene surface by transferring the CVD graphene onto biomimetic microstructured Al [59] and iron [60] alloy substrates and obtained WCAs > 130°.

For the CVD graphene, Cu is the most-used substrate for graphene growth [17], and the wettability of SLG/Cu has been widely investigated [61-63]. Cu with clean and non-oxidized surface is highly hydrophilic [64] while the cover of graphene significantly increases its WCA [52, 62]. Recently, with the comprehensive characterizations on the structure and morphology of Cu substrates before and after the graphene growth, researchers have found that the wettability of graphene/Cu is closely related to crystal planes, grain sizes and surface roughness of the Cu substrates. Additionally, the uneven synthesis of graphene in large areas and its local separation from Cu are also accountable for the increased WCA of SLG/Cu in comparison with the predicted values. S.Y. Misura *et al.* conducted systematic studies to understand how these factors impact the wettability of the CVD graphene on Cu prepared [61] and reported that the graphene on the textured Cu surface is usually more hydrophobic than that on the smooth Cu surface [65]. After conducting MD simulations to compare the wettability of SLG on Cu(111), Cu(110) and Cu(100), they further found that SLG/Cu(111) is most hydrophilic while SLG/Cu(110) is most hydrophobic (Figure 3h) [66]. Except for the graphene directly grown on Cu, for graphene transferred on various substrates, the influences of the structure disturbance on its wettability are also widely reported. For example, Evelyn N. Wang *et al.* found that the loose interlamellar coupling between the transferred graphene and the substrate results in large interlayer space, which in turn weakens the effect of the underlying substrate on the graphene wettability, making the wettability of graphene more like that of the graphite [67]. Besides, the wettability differences of substrates before and after graphene coating can also be employed for the non-destructive, fast visualization of isolated graphene domains [68]. This is compatible with different types of substrates, such as SiO_2, quartz, glass, Cu, Si, Au, and PDMS (Figure 3i, j).

To investigate the intrinsic wettability of the pristine graphene experimentally, the influences of substrates have been experimentally excluded thanks to the successful preparation of large-area free-standing graphene and the utilization of novel wettability measurement techniques. In 2018, Grégory F. Schneider *et al.* fabricated millimeter-scale freely suspended graphene by injecting an air bubble underneath a SLG floating at the water–air interface (Figure 4a, b) [43], and found that the free-standing clean graphene is hydrophilic with a WCA of

42° ± 3° (Figure 4c). The same group also reported that graphene is strikingly hydrophilic with a WCA of 30° ± 5° on ice and 10° ± 2° on hydrogel and concluded that graphene is transparent to both polar and dispersive interactions (Figure 4d) [42]. In 2021, Zhongfan Liu *et al.* prepared circle-shaped suspended graphene using a holey substrate to exclude the impact of underlying substrate and measured its WCA using a high-resolution environmental scanning electron microscope (ESEM) (Figure 4e, f) [41]. They concluded that the unsupported graphene is hydrophilic with an average WCA of 30°, which is independent of the tilt angle of the ESEM sample holder, and the droplet size (Figure 3g, h). These results further demonstrate the intrinsic hydrophilicity of pristine graphene.

2.3. Impact of surface contamination on graphene wettability

Notably, surface contamination is the main reason for the long-standing controversy about graphene wettability [41], given that it has been reported to increase the WCA of graphene, making it more hydrophobic. Based on the origin, the contamination on the surface of CVD graphene can be classified into three types, including intrinsic contamination (amorphous carbon) formed during the high-temperature growth process, polymer residues introduced during the transfer process, and airborne hydrocarbon contamination adsorbed during storage [19, 69, 70].

After elucidating the origin of the intrinsic contamination on the graphene surface and developing strategies to synthesize superclean graphene [20, 71, 72], Zhongfan Liu *et al.* observed that the superclean graphene film grown on Cu(111) single-crystal surface has a much smaller WCA (35°), in comparison with that of the unclean graphene (64°) (Figure 5a, b) [64]. By employing the pentagon and heptagon carbon rings as the simplified structures of the intrinsic contamination (amorphous carbon) for MD simulations, they confirmed that the appearance of amorphous carbon contamination results in a larger WCA (Figure 5c) for both the suspended and supported graphene. This can be attributed to the decreased adsorption energy of water molecules (Figure 5d) and the formation of Cassie–Baxter wetting state on the unclean graphene surface. Moreover, the transferred unclean graphene transferred is still more hydrophobic than its clean counterpart. For instance, the clean SLG/quartz has a smaller WCA (~ 40°) than that of the unclean SLG/Cu (~ 70°) (Figure 5f). This group also observed that the unclean suspended graphene prepared using a poly(methyl methacrylate) (PMMA)-assisted transfer method is more hydrophobic that the suspended clean graphene prepared via a polymer-free transfer method, indicating the impact of transfer-induced polymer residues (Figure 5e).

Haitao Liu *et al.* in 2012 reported the impact of the adsorbed airborne hydrocarbon on the graphene wettability by measuring the temporal WCAs on graphene after taking it out from the CVD chamber [73]. They found that the WCA is 44° on the fresh graphene and increases sharply to 60° within 20 mins when exposing the graphene to air. The adsorption of hydrocarbon is confirmed by attenuated total reflectance Fourier-transform infrared spectroscopy, which shows the symmetric and asymmetric stretching of the methylene group (-CH_2-) at 2,850 cm^{-1} and 2,930 cm^{-1} respectively. The integrated areas of the two stretching peaks increase monotonically with the exposure time, proving the accumulation of hydrocarbon contaminations, further confirming the striking effects of the airborne contamination on the graphene wettability. Being proportional to the surface coverage of the adsorbed contaminants, the WCA value ceases to change when the adsorption saturation is reached. After that, the as-formed more hydrophobic graphene surface can maintain long time, as indicated by the long-time stability of graphene wettability: negligible WCA changes for SLG on mica, quartz, TiO_2, SiO_2, Si, Au, PET and Cu substrate were observed after 14 months (Figure 5g) [63]. In the past decade, Haitao Liu's group has conducted systematic studies in these fields using graphene, graphite [37, 51, 70, 74, 75] and similar phenomena have also been reported experimentally by other groups [76-80].

To fully understand the effect of hydrocarbon contamination on graphene wettability, MD simulations have been extensively conducted. N. R. Aluru *et al.* employed ethane molecule as the simplified structure of the

hydrocarbon contamination and observed an obvious increase of WCA with the contamination density when using three types of carbon−water interaction parameters, suggesting the high sensitivity of graphene wettability to the surface contamination [81]. Herbert M. Urbassek *et al.* observed similar change when putting ethane atop the graphite substrate [77]. Alenka Luzar *et al.* utilized butylated graphane (a saturated derivative of graphene) to simulate the wetting state of contaminated graphene and confirmed that the wetting transparency of graphene is essentially insignificant when coating ~ 5 Å hydrocarbon [82]. Sokrates T. Pantelides *et al.* utilized methane molecule as the simplified structure of the hydrocarbon contamination and found that the presence of contamination decreases the water density near the graphene (Figure 5h), thus weakening the interactions between graphene and water molecules, making it more hydrophobic [45].

3. Tunability of graphene wettability

Structural factors, such as defects, layer numbers, wrinkles, and doping, play a crucial role in determining the graphene wettability by directly influencing the water-graphene interactions [21, 22]. In this section, we will provide a comprehensive overview of the key structural factors that affect the wettability of graphene, as well as the main methods used to regulate the wettability.

3.1. Defect

In comparison with exfoliated graphene flakes, large-area CVD graphene films unavoidably have more defects, especially considering the complex transfer process [83]. Therefore, it is important to understand the impact of different types of defects including point defects (such as vacancy), and line defects [such as grain boundary (GB) and wrinkles], on the graphene wettability.

Xiufang Bian *et al.* studied the wetting states of water droplets on four types of graphene: defect-free and with Stone-Wales (SW), single-vacancy (SV), double-vacancy (DV) defects (Figure 6a, b) [84]. They found that the influences of these defects are limited with the WCA change < 7° (Figure 6c), which might be because that the point defects can only induce the small surface fluctuations and charge transfer change in a limited size. SungWoo Nam *et al.* compared the WCA of perfect and defective graphite, and concluded that the WCA change caused by losing carbon atoms to form 4.2% SV, DV, SW defects is < 15°, indicating that the electrostatic interaction between the water dipole and graphene attributable to local charges at these defective sites is weak [85]. When H atoms chemically adsorb on these defective sites, WCA increases by ~ 5°. However, when OH bond forms at these vacancy sites, WCA decreases significantly to < 10° (Figure 6d). In 2017, Lei Li *et al.* reported that graphite surfaces with different defect densities, always have similar advancing WCA values, but very different static and receding WCAs [86]. Masumeh Foroutan *et al.* demonstrated that the WCA on the perfect graphene is smaller than that on the penta-graphene, a two-dimensional allotrope of carbon with coplanar pentagonal rings, which can be attributed to less hydrogen bonds formed between water molecules and the penta-graphene [87].

Chang et al. investigated the impact of the graphene GBs and found that with the average graphene grain areas increasing from 0.47 mm^2 to 22.16 mm^2, the static WCA on polycrystalline graphene surfaces increases from 47.9° to 68.8°, accompanied by the decrease of the hysteresis WCA from 45.9° to 32.7° (Figure 6e) [88]. This is mainly caused by the inhomogeneous wetting, as identified by the pinning contact lines of nucleated micro-scale droplets along the GBs as revealed by ESEM. Their ESEM results also pointed out that the Cu GBs have less influence on the graphene wettability than the graphene GBs.

Graphene wrinkles, which can be formed during both the CVD graphene growth and transfer process [89-91] and have varied height (from sub-no to tens of nm) and width (from sub-nm to tens of nm) [92-94], can be recognized as another type of line defect. With dense distribution, the graphene wrinkles have significant

influences on the graphene wettability. By stacking isolated graphene layers atop the SLG/Au, Siddhartha Das *et al.* demonstrated that the roughness-induced chemical heterogeneity leads to a larger WCA of graphene/Au (~130°) than that of both SLG/Au (75°) and bilayer graphene (BLG)/Au (91°) [95], resulting from contact line-pinning-driven hydrophobicity caused by the wettability gradient on graphene-nanostructure-coated substrates (Figure 6f). Wen-Ming Zhang *et al.* fabricated conformal graphene wrinkles with bilayer systems of PMMA and PDMS [96]. They observed that the wrinkled graphene (WG) is more hydrophobic, as proven by a large WCA over 126°, while the WCA of the flat or unwrinkled graphene supported by PMMA-PDMS is ~ 106° (Figure 6g, h). A more hydrophobic surface of the WG grown on copper–zinc alloy substrates using CVD method has also been observed by Hongwei Zhu *et al.* [34, 97].

3.2. Layer number

The wetting state of graphene changes with its layer number, which is often discussed together with the wetting translucency of graphene, since the multilayer graphene (MLG) with layer number N can be seen as the SLG supported by (N-1) graphene layers [52]. Considering the effect of the substrate underneath, the WCA evolutions of the suspended and supported graphene with its layer number are different and thus discussed separately.

When investigating the wettability of the suspended graphene, vdW interactions between water molecules and graphene are normally considered as the dominant factor. In 2012, Daniel Blankschtein *et al.* developed the first theory to model the vdW interactions between liquid and graphene [53], based on which they simulated the WCA change with the graphene layer number (N) under the assumption that vdW interactions dominate the interactions between the water and graphene surface. They found that when N < 10, WCA decreases rapidly with N, accompanied by a rapid increase of the vdW potential per unit area between graphene and water ($-\Phi_{NL}$). When N > 10, the change of the calculated WCA becomes negligible (Figure 7a), in good agreement with the work reported by Haitao Liu *et al.* [73]. In 2013, N. R. Aluru *et al.* developed nonbonded interaction parameters between graphitic carbon and water entirely from *ab initio* calculation data of interaction energies of water monomer above graphene, followed by MD simulations to investigate the impact of layer number [81]. They found that that SLG has a larger WCA than BLG and tri-layer graphene (TLG). Moreover, the WCA difference between BLG and TLG is much smaller than that between SLG and BLG. In 2018, Sokrates T. Pantelides *et al.* demonstrated a similar decreasing trend of WCA as a function of the graphene layer number via MD simulations, based on the assumption that the dispersive interaction between graphene and water molecules dominates the wetting behaviors [45]. In 2021, Paola Chiricotto *et al.* studied the interfacial energies and wetting properties of graphene with different layer numbers, from N = 1 ~ 3 to N = 6, in two systems, namely, a fully wetted one with water in both sides and a partially wetted one for which only one side contacts water [98]. They found that the graphene becomes less hydrophobic when increasing the layer number in both systems and attributed this to the combined effect of (1) the electrostatic interactions between the water molecules, (2) the vdW interactions between water and graphene and (3) the vdW interactions between the water molecules. Recently, a same trend has been observed experimentally using ESEM [99].

For the wettability of the supported graphene, the effect of its layer number needs to be considered together with the effect of underlying substrates, which usually increases the polar interactions with water molecules [100, 101]. Most reports highlight the increased hydrophobicity of graphene with thickness from both experiments and simulations. Some representative works are discussed below. In 2012, using both MD simulations and classic model, Nikhil A. Koratkar *et al.* reported that with the increased layer number of graphene on Cu, the adsorption energy of water molecules decreases and the WCA increases [52]. At the same time, they also measured the WCA of graphene on Cu and glass substrates with different layer number, which provides same conclusion as their simulations, in good agreement with the results reported by several other

groups [67, 102, 103]. In 2013, Evelyn N. Wang *et al.* further investigated the effect of the layer number on the dynamic wettability of graphene by measuring the advancing and receding WCAs of SLG, BLG and TLG on Cu, SiO_2 and glass substrates. They found that only the advancing WCA could truly represent the wettability of graphene-coated surface while the receding WCA is significantly influenced by intrinsic defects [67]. Their MD simulations demonstrated that for graphene on Cu substrates, WCA increases with layer number until it approaches the WCA value of HOPG. However, on SiO_2-hydroxylated surface, the WCA has little dependence on layer number and is comparable to that of HOPG. In 2018, Jianxiang Wang *et al.* calculated the polar, dispersive and total energy of bare glass and the graphene (1-3 layers) coated glass substrates, finding that the polar surface energy of glass decreases sharply with the increased number of graphene layers (Figure 7b, c) [55]. In 2022, Minhaeng Cho *et al.* investigated the water-graphene interface using MLG on hydrophilic calcium fluoride (CaF_2) by vibrational sum-frequency-generation (VSFG) spectroscopy [102]. The WCA on CaF_2 is 22.3°, increases sharply to 53.1° and 79.6° after SLG and TLG coating, and finally stabilizes when the layer number further increases to six (Figure 7d). The authors also measured the self-defined VSFG wettability by using the areas of strongly H-bonded OH, weakly H-bonded and dangling OH peaks for establishing the molecular origin of the wettability of MLG by detecting the spectra of specific bonds (Figure 7e). Additionally, for the CVD graphene directly grown on dielectric substrates, it is also widely observed that thicker graphene is more hydrophobic. For instance, Zhongfan Liu *et al.* observed WCA increases with the thickness for both *n*-doped graphene grown on glass [104] and pristine graphene directly grown on flexible glass substrate (Figure 7f), indicating a tailorable surface hydrophobicity of the graphene/glass [105].

3.3. Doping

The doping in graphene can be classified into four types: underneath substrates, continuous external electron flows, heteroatoms in graphene lattice, and surface functional groups. Both *n*- and *p*-type doping of graphene have been reported to make graphene more hydrophilic, primarily due to the modulation of charge carrier density (Figure 8a) [106, 107].

WCA differences for graphene supported by different substrates are commonly observed [37, 68]. Ali Ashraf *et al.* reported the tunable graphene wettability through substrate doping, using different subsurface polyelectrolytes, such as poly(allylamine hydrochloride), poly-L-lysine for *n*-doped graphene and poly(sodium 4-styrenesulfonate) and poly(acrylic acid) for *p*-doped graphene [106]. They achieved a maximum WCA change of 13° when the doping level changed by 300 meV. Additionally, they found that a lateral metal-graphene heterojunction or subsurface metal doping could induce such wettability modulation, which can be attributed to the modulated binding energy between water and graphene. Note that the metal doping and corresponding WCA change of graphene is closely related to their work functions [108].

Guo Hong *et al.* observed enhanced hydrophilicity when they shifted the Fermi level of graphene away from its Dirac point via electrical voltage doping by applying a direct current (DC) voltage bias to a graphene film on a SiO_2/Si substrate [109]. This is because water molecules preferentially orient themselves under electron- or hole-rich conditions to form more energetically favorable configurations, which leads to a stronger interaction between water and graphene thermodynamically, in turn reducing WCA. The tunable and reversible WCA on graphene transferred onto flexible transparent substrates, such as polyethylene terephthalate (PET) and PDMS has also been achieved after applying gate voltage (Figure 8b) [110]. This phenomenon is named as electrowetting [110-112].

Heteroatoms, such as N, B, P, S, O, and metal (e.g., Pt, Fe) atoms, can replace C atoms in graphene lattice via either direct CVD synthesis or post-treatment, leading to the formation of doped graphene [113, 114]. For example, by using ethanol and methylamine as the precursor and dopant, respectively, Zhongfan Liu *et al.* acquired predominantly graphitic-N-doped graphene with a relatively smaller WCA [104].

Surface functionalization, which is very popular for doping graphene, is achieved primarily through post-treatment techniques [115], and can be broadly classified into wet and dry methods, depending on whether liquid, especially water, participates the doping process [116]. Wet methods involve the use of chemical solutions, resulting in covalent or non-covalent doping of graphene, depending on whether its lattice is damaged. For example, Hongwei Wang *et al.* chemically modified SLG to link bioactive ligands to its basal plane through covalent functionalization by immersing the samples in the solution, thus generating a hydrophilic surface (Figure 8c) [117]. To maintain graphene's exceptional properties while changing its wettability at the same time, non-covalent doping is preferred, to achieve which aromatic compounds are usually utilized [118]. For instance, Mikito Yasuzawa *et al.* utilized 1-pyrenebutyl-2-(trimethyl-ammonium)ethyl phosphate to modify graphene surface (Figure 8d) [119] and Philippe Buhlmann *et al.* demonstrated non-covalent monolayer modification of graphene using pyrene and cyclodextrin receptors [120]. Last year, Fatima Bouanis *et al.* reported the functionalization of graphene using different kinds of aromatic molecules through π-π interactions, such as Fe-/Co-porphyrin and Fe-phthalocyanine [118].

Dry methods for doping graphene mainly include plasma treatment, ion bombardment, thermal annealing, and UV/ozone treatment, which typically start from cleaning the graphene surface, followed by destroying the graphene lattice to form covalent bonds between the C atoms in graphene and the introduced external atoms or functional groups, such as COOH, -OH, NH_3- [11, 116]. To generate plasma, N_2 [121], Ar [122], O_2 [69, 123, 124], H_2 [125] and their mixing gases are often utilized (Figure 8e), to change the Fermi level of graphene and accordingly its wetting states, accompanied by the optimization of parameters including power, pressure, flux and treatment time. For instance, Okada *et al.* generated the *n*-doped graphene using N_2 plasma generated by a neutral beam system, decreasing WCA by ~ 15°. Jongill Hong *et al.* obtained a hydrophilic graphene (WCA~16°) surface after a hydrogeneration treatment for 700 seconds [125]. Cheng Yang *et al.* decreased the WCA of graphene on SiO_2 from 48° to 30° via Ar plasma treatment [122]. Hailin Peng *et al.* decreased the WCA of graphene for over 40° after 40 s O_2 plasma treatment (Figure 8f) [69]. UV/ozone treatment is another option to functionalize graphene, which is efficient for the surface cleaning and defect engineering of graphene [126]. The WCA of SLG/Cu decreased significantly from ~ 90° to ~ 30° through ozone treatment [126, 127]. Moreover, the WCA of SLG on ITO-coated glass decreased from ~ 76° to ~ 13° (Figure 8g) after the ozone treatment, which can be attributed to the increased polar interactions in the surface energy of the oxidized graphene (Figure 8h) [128]. The atmosphere also influences the wettability change rate and final WCA values when the ozone treatment is conducted (Figure 8i) [76].

4. Application of graphene in energy fields

Graphene has drawn tremendous interests over the past two decades as a material that can promote the development of energy generation, storage, transduction, and harvesting [11, 13, 129, 130]. Graphene oxide, reduced graphene oxide, and graphene flakes produced through exfoliation methods have been extensively used thanks to their low cost and fine scalability [13, 130-132]. However, the abundance of defects, small flake size, and varied layer number in these materials limit their properties compared with high-quality CVD graphene films [133]. The latter exhibits superior properties in terms of high transparency, electrical conductivity, mechanical strength, thermal conductivity, impenetrability, and tailorable wettability [133], making it advantageous for broader energy-related applications. The past decade has witnessed a rapid development of scalable production and transfer techniques for CVD graphene, making it more accessible for both academia and industry [17]. In this section, we discuss the water-involved energy applications of CVD graphene, such as solar cells, supercapacitors, batteries, nanogenerators, heat transfer, defoggers, and water harvesters by clarifying the function of graphene, especially the significance of graphene wettability for improving the device performance.

4.1. Solar cell

Solar cells are an important technology for renewable energy generation. To make the best use of CVD graphene, both graphene-silicon Schottky junction solar cells and graphene-involved perovskite solar cells (PSCs) have been extensively investigated [131, 134, 135].

Solar cells based on the Schottky junction between graphene and silicon provide a promising alternative to silicon diode-based solar cells, owing to their low cost and facile process, where the graphene acts as both a transparent electrode and an active layer [136-138]. By doping graphene with bis(trifluoromethanesulfonyl)-amide, a power-conversion efficiency (PCE) of 8.6% is obtained, which is much higher than that obtained using the undoped graphene (1.9%) [23]. At the same time, the increased work function of graphene results in an increased voltage drop at the Si/graphene interface, leading to a more efficient separation of electron-hole pairs to generate useful current. Especially, the hydrophobic surface of the doped graphene contributes to a superior environmental stability of the device, in comparison with the undoped one.

For PSCs, graphene can be employed as the charge transport layer, electrodes, stabilizer, or interface layer, for improving efficiency and long-term stability [131, 139]. However, given the diverse structures of PSCs and different roles of graphene, the requirement for wetting states of graphene varies in different scenarios. For instance, to ensure long-term stability, a hydrophobic surface is necessary to protect perovskite materials from degradation, especially in humid atmospheres. A relatively hydrophilic surface is preferred, however, when the graphene is used as the charge transport layer to grow high-quality perovskite films for efficiency improvement, since the wettability and roughness of graphene significantly impact the morphology and crystallinity of the perovskite [134, 140]. The tunable wettability of graphene is also critical in guaranteeing an ideal interface charge transfer process. In 2015, Sung *et al.* reported the use of CVD graphene as bottom electrodes in inverted structure PSCs by transferring graphene from Cu onto a glass substrate (Figure 9a) [24]. However, with the WCA of poly(3,4-ethylenedioxythiophene): poly(styrenesulfonate) solution on graphene being ~ 90.4°, the hydrophobic surface of the transferred graphene makes it challenging to deposit high-quality poly(3,4-ethylenedioxythiophene): poly(styrenesulfonate) atop. To address this issue, an ultrathin MoO_3 layer (1-4 nm) was deposited on the graphene surface via vacuum thermal evaporation, leading to a significant decrease in WCA (46.6° for 1 nm thick MoO_3 and 30° for 2 nm thick MoO_3) (Figure 9b, c). This, in combination with the efficient increases in both the work function and electrical conductivity of the graphene, resulted in an obvious efficiency improvement in comparison with its counterpart without the MoO_3 deposition (Figure 9d). Besides, to play a good role in PSCs, the CVD graphene has been doped using many other ways, all of which change its electrical properties and wetting states at the same time, contributing to the enhanced device performance [23, 128, 141-146].

4.2. Battery and supercapacitor

Though graphene have found widespread applications as electrodes, conductive additives, or current collectors in both batteries and supercapacitors, the atomic-thick CVD graphene films are only suitable to function as a surface modification layer or interphase, rather than replacing the current components [130, 132]. For example, a wax-assisted transfer method has been used to transfer the inert high-quality CVD graphene onto Li foil to serve as an artificial solid/electrolyte interphase (Figure 9e) [25]. With a WCA of ~ 107°, the graphene layer could passivate the Li surface from moisture erosions and side reactions and help guide the homogeneous Li plating/stripping, suppressing the dendrite and formation of ‘dead’ Li. As a result, the Li-air batteries made with passivated Li anodes exhibit superb cycling performance up to 2,300 hours, indicating extraordinary air and electrochemical stability (Figure 9f). Additionally, a hydrophilic graphene surface is generally required in aqueous electrolyte systems to increase the contact area and guarantee effective charge

transfer [147] while for metal-air batteries[148], such as Li-air and Zn-air batteries, appropriate hydrophilicity is vital for balancing the reaction rates on gas-solid and gas-liquid interfaces [149-151]. For example, Huanxin Li *et al.* reported that the use of graphene is able to guide the homogeneous Zn plating/stripping, suppressing the formation of dendrite in Zn-air batteries [152].

Supercapacitors have attracted extensive attention as energy storage equipment because of its high-power density, long life, and acceptable energy density [153]. The participation of CVD graphene in electrical double layer capacitors (EDLCs) by altering the charge distribution and transfer in the liquid-electrode interface has been investigated [26, 154, 155]. EDLCs consist of two parallel layers of opposite charges and rely on the formation of the electrical double layer (EDL) to store energy. SungWoo Nam *et al.* investigated the influence of the graphene wettability on EDL formation and found that both the area-normalized total capacitance (C_T) and the normalized transconductance (g_{nm}) decrease with the increase of WCA on graphene [156], indicating a disruption of the EDL formation due to the hydrophobicity and thus the preference of hydrophilicity to improve the capacitance. Kefa Cen *et al.* reported that the graphene wettability can significantly alter the microscopic electro-sorption of electrolytes, including ions and solvent molecules, thus affecting the formation of the interfacial EDL microstructure and energy storage capability [27]. They studied the electrolyte electro-sorption within both non-confined and confined spaces via numerical simulations (Figure 9g). For the former, capacitance decreases monotonically with increasing hydrophilicity (Figure 9h) due to the strong electro-sorption of solvents at the interface rather than ions, while for the latter, non-monotonic dependence on the graphene wettability (i.e., an asymmetric bell-shaped curve) is observed (Figure 9i), challenging long-held axioms, and indicating the complexity of real electrochemical systems. Till now, experiment research using CVD SLG in supercapacitors is still in its infancy, which might be inspired by above simulation results.

4.3. Nanogenerator

In recent years, graphene-based hydro-voltaic technology using the SLG has emerged with its promising potential for energy harvest by generating electricity from various water sources, including rain, flows, waves, moisture, and natural evaporation [12, 13].

In 2011, Niknil Koratkar *et al.* first reported energy harvesting from water flow over graphene [157]. They measured a power output of ~ 85 nW for a graphene film of 30 * 16 μm^2 in size, which is equivalent to a specific power output of ~ 175 W/m^2. In 2012, Wanlin Guo *et al.* found that exposing graphene and its metal electrodes to solutions simultaneously could induce a voltage from a few to hundreds of millivolts while no electricity can be generated if only graphene is exposed to solutions [158]. Subsequently, they demonstrated the electricity generation by moving a droplet of ionic liquid along graphene (Figure 10a) [28] or moving graphene sheets in the ionic liquid (Figure 10b) [159]. In addition to collecting electricity from graphene, they also transferred a pair of graphene sheets onto PET substrates to harvest the electricity generated in liquid, obtaining an open circuit voltage up to 1.0 V [160]. In these works, the ion species (e.g., H^+, Li^+, Na^+, K^+, Mg^{2+}, Cl^-, Br^-, I^-, etc.), concentration (0-1 M), and velocity (up to 40 cm/s) are the main factors that influence output voltage and current, while the advancing and receding CAs remain nearly unaffected by the ion species, except for HCl [28].

The support substrate for graphene is crucial for electricity generation because it plays a dominant role in attracting ions to the water/graphene interface. Shisheng Lin *et al.* obtained a direct current electricity with voltage of ~ 0.3 V from a dynamic polarized graphene-water-silicon interface (Figure 10c) [161]. Chuanshan Tian *et al.* found that the surface dipole layer of PET or polyvinylidene fluoride (PVDF) is responsible for the ion attraction towards adsorption at the graphene surface (Figure 10d) [7]. However, PMMA, which has negligible ion attraction ability, cannot contribute to electricity generation, since graphene itself does not attract ions and only acts as a conducting layer for the induced carrier transport. Moreover, after systematically

investigating the synergistic effect of the substrate and ion liquid, Wanlin Guo *et al.* found that the electronegativity of substrates influences the doping states of graphene, which, in turn, can significantly enhance the charge transfer on graphene [162]. Currently, the output voltage of SLG-based nanogenerators ranges from sub-mV to nearly 1 V, with output currents at the level of 1-10 μA. However, in most application scenarios, graphene is transferred from Cu onto functional substrates, which increases process complexity and suffers from the weak interactions between graphene and the substrate underneath. To address this problem, the direct growth of graphene on the target substrates has more advantages. Zhongfan Liu *et al.* reported that the droplet-based hydro-voltaic electricity generator device fabricated using graphene film directly grown on glass shows more robust voltage output and enhanced long cyclic stability compared with the one fabricated using the transferred graphene (Figure 10e, f) [163].

Piezoelectric and triboelectric nanogenerators are widely used for harvesting hydropower using graphene. In 2016, Shisheng Lin *et al.* reported a graphene-piezoelectric material heterostructure for harvesting energy from the water flow and obtained an increased power output of ~ 1.9 μW, which is a hundred times higher than previously reported results (Figure 10g) [164]. The introduction of a piezoelectric template, polytetrafluoroethylene (PTFE) beneath graphene, enables a continuous charging-discharging process in graphene, resulting in an obvious voltage output up to 0.1 V even with distilled water. Sang-Woo Kim *et al.* reported the triboelectrification-induced large electric power generation from a single moving droplet on graphene/PTFE (Figure 10h) [164]. Series and parallel connection of three individual graphene/PTFE structures were also conducted to increase either the output voltage or current. In 2022, Zhonglin Wang *et al.* put forward with an effective strategy via interface lubrication to enhance the direct-current density and lifetime of the triboelectric nanogenerator simultaneously using water-based graphene oxide solution as a lubricant and CVD SLG as the electrode materials (Figure 10i, j) [29].

Moisture and evaporation-induced electricity generation is an alternative method for producing clean and sustainable energy. A recent research by Hongwei Zhu *et al.* has demonstrated a highly efficient humidity-driven electric nanogenerator based on the interfacial cation-π interaction by using the highly WG with intentionally increased defects and uniform distribution [97]. Electric energy generation is achieved through the transformation between ionic liquid microdroplets and salt crystals via water adsorption and desorption as humidity changes. This is because compared with flat graphene films, WG is more hydrophobic, thus allowing ultrafast water evaporation and preventing excessive water accumulation (Figure 10k, l).

4.4. Heat transfer

With its high thermal conductivity and tunable wettability, graphene shows great advantages in both condensation heat transfer and boiling water heat transfer.

The condensation heat transfer occurs when the surface temperature is lower than the dew point of the moist air and can be classified into two types: dropwise condensation for hydrophobic surfaces and filmwise condensation for hydrophilic surfaces. To enhance the heat transfer, dropwise condensation is preferred, indicating the significance of preparing a hydrophobic surface. In 2015, Daniel J. Preston *et al.* reported a four-times enhancement of the condensation heat transfer by using the CVD SLG directly grown on the Cu condenser tube [30]. This enhancement is mainly attributed to the hydrophobic surface after graphene coating with an advancing WCA > 80° and receding WCA > 50° (Figure 11a-d). The excellent chemical stability and high thermal conductivity, that is, low thermal resistance of graphene further contribute to the superior performance of the SLG-modified Cu condenser. Recently, the performance of the condensation heat transfer has been further enhanced by using a functionalized-graphene coating, which is more hydrophobic than the pristine graphene and thus can facilitate the movement of droplets on the surface (Figure 10e) [165]. Besides, Wei Chang *et al.* recently achieved a sustainable dropwise condensation and effective heat transfer by using the FLG

grown on Ni substrate via CVD [166].

The boiling heat transfer, which accompanies the latent heat transfer of the working fluid, is considered as the most efficient cooling methodology due to the low wall superheat. In 2019, Ji Yong Kim *et al.* combined CVD SLG with the highly wettable FC-72 for a boiling heat transfer experiment and demonstrated the advantages of graphene in enhancing both the heat transfer coefficient and critical heat flux, the two key parameters related to the performance of boiling heat transfer [167]. In 2020, Ching Yuan Su *et al.* confirmed the advantages of the fluorinated graphene as atomic layered modifiers for enhancing pool boiling heat transfer (Figure 10f) [31]. Along with the bubble dynamic visualization, they found that the increase of CA leads to more active cavities, which plays a vital role in heat transfer (Figure 10g). By using the fluorinated graphene coating on a plain copper surface and nonpolar refrigerant R-141b as the working fluid, they achieved twice enhancement of the heat transfer compared with the pristine graphene (Figure 10h).

4.5. Defogger and water harvester

Graphene has great potential in applications of water harvesting and defogging, both of which favor a hydrophobic surface. Gun-Tae Kim *et al.* studied the impact of the Cu substrate topography on the evaporation of water droplets on the Cu-supported graphene by tailoring its wettability [32]. In specific, after synthesizing SLG on a hydrophobic electroplated Cu surface which is rough and makes the SLG/Cu surface hydrophobic, they observed the accelerated water condensation and fast water harvesting through dehumidification (Figure 12a, b). Kang Liu *et al.* achieved a 40-100% enhancement in condensation efficiency for a 5 hours' vapor condensation at a subcooling of 40 ^{o}C using the graphene modified PDMS substrate. This can be attributed to the wetting transparency of graphene, which means that the wetting behavior of the structured hydrophobic surface of PDMS is not significantly disturbed by the graphene coating. The graphene coating also prevents the moisture from reaching the structure gaps and thus impeding Cassie-wetting failure of the surface [168].

SLG and FLG films have been utilized as defoggers on dielectric substrates, such as quartz and sapphire, thanks to their high electrical and thermal conductivity, together with hydrophobicity (Figure 12c, d) [33, 169, 170]. The applied voltage typically ranges from 10 V to 40 V, and the defogging time decreases accordingly, ranging from several seconds to several minutes. Notably, directly grown graphene exhibits higher stability in long-term cycle experiments compared with transferred graphene (Figure 12e), which is mainly due to the strong interactions formed between the growth substrates and graphene [171, 172]. In addition to flat graphene films, Hongwei Zhu *et al.* achieved the fast defogging and anti-icing using the WG (Figure 12f), which has a WCA of ~ 87^{o} (Figure 12g) and ~ 91^{o} on Si wafer and glass, respectively [34]. The special structure of the defective WG effectively prevents the water gathering and promotes the water evaporation, avoiding excessive water accumulation (Figure 12h, i). As a result, the WG-based defogger exhibits relatively lower input voltage and good robustness (Figure 12j). Fog can be completely removed within 5 s when a safe voltage of 28 V is supplied. Moreover, since the resistance of the defoggers is sensitive to humidity, real-time monitoring of the defogging process is also achievable in this work.

5. Summary and perspective

This review provides the recent research progress on the graphene wettability, elaborating the water-graphene interactions and clarifying the impact of the underlying substrates together with the surface contamination on graphene wettability. The main structural factors that affect the wettability of the CVD graphene are then discussed, accompanied by the versatile graphene growth, transfer, and post-treatment methods developed to change the structure of graphene and thus its wettability. The latest advances in energy applications including solar cells, supercapacitors, batteries, nanogenerators, heat transfer and water harvesting,

of the CVD graphene with its tunable wettability are also summarized. Finally, we present a summary and perspective to indicate the future directions for the practical applications of the high-quality CVD graphene in these energy fields.

When comparing CVD graphene with graphene flakes produced via reduction of liquid exfoliated graphene oxide in terms of wettability, there are some clear differences and common behaviors, which will be discussed separately below. For the former, CVD graphene exhibits distinct, structure-dependent wettability behaviors, making it an ideal platform for fundamental research. The wettability of CVD graphene is closely linked to that of the substrates, with measured WCA values typically smaller than those for graphene derived from graphene oxide due to significantly reduced defect density and surface functional groups. On the other hand, for the latter, the wettability of both types of graphene can be readily adjusted over a wide range, from hydrophilic to hydrophobic, and the coating process for both samples is highly contingent on the wettability of both the target substrates and the material itself. To date, in the field of energy applications, liquid-exfoliated graphene flakes have been widely utilized due to their ease of production and cost-effectiveness. However, with the rapid advancements in the mass production of CVD graphene, increasing attention has been directed toward CVD graphene because it offers unique advantages such as high transparency, exceptional electrical conductivity, high thermal conductivity, and large-area uniformity. Overall, both types of graphene present distinct characteristics in terms of wettability, with each finding its niche in various applications based on their specific attributes.

It is evident that the adoption of the high-quality CVD graphene with tunable wettability in energy fields is advantageous. However, several challenges need to be overcome to increase the competitiveness of water-involved energy devices that utilize CVD graphene. Firstly, the scalable production of graphene with high consistency is crucial to lower the cost. Secondly, novel graphene transfer methods compatible with different functional substrates and device fabrication processes are required. For example, in PSCs, the perovskite materials are very sensitive to both organic and inorganic solvents. Thirdly, to enhance the stability of the graphene-based devices, graphene needs to be tightly adhered to the underlying substrates, for which the direct growth of graphene on the target substrates is the best option. However, since most of the non-metal substrates are catalyst-free or not stable at high temperatures, novel CVD growth strategies to improve graphene quality, controllability, as well as uniformity or to decrease the growth temperature are still required. Meanwhile, scalable, and simple post-treatment methods are still required to tune the graphene wettability or widen the WCA range, especially those environmental-friendly, vacuum-free, dry ones. Moreover, modulation of wetting states of graphene to both superhydrophilic and superhydrophobic range will enlarge its generality in various energy fields.

There are various methods for evaluating the wettability of graphene, most of which rely on directly measuring the static WCA. This is relatively straightforward when dealing withCVD graphene supported by a substrate. However, assessing the intrinsic wettability in pristine graphene poses great challenges, primarily owing to the preparation of suspended graphene and the following special setup required, such as conducting ESEM measurement using tilted sample holder to record water droplets shaper on suspended graphene, and measuring the shape of bubble underneath mm-sized graphene floating on water. Furthermore, dynamic WCA measurements offer more comprehensive insights by capturing advancing and receding contact angles, as well as their hysteresis. To directly analyze the shape of small water droplets on graphene, Cryo-SEM proves helpful, allowing for the observation of frozen water drops on graphene. AFM and TEM are also viable options for investigating graphene's wettability through the fabrication of graphene-based liquid cells. While WCA quantifies surface wettability on a macroscopic scale, nanoscale wettability is assessed through the measurement of adhesion forces using AFM, which involves tracking the attractive maximum in the force profile. In recent developments, VSFG has been employed to elucidate the water structure at the graphene-water interface. This characterization might also be achieved through the utilization of Cryo-TEM.

The systematic investigation into the role of graphene in energy devices is still in its infancy but is imperative. To make the best use of the CVD graphene in accelerating the development and utilization of water-based clean, renewable energy, special attention could also be paid to the following aspects. Generally, the electronic, thermal, and mechanical properties of graphene are altered when tuning its wettability through doping or surface modification, which needs to be taken into consideration when analyzing the device performances and might inspire more interesting applications of graphene. The excellent properties of pristine graphene are advantageous in many applications. However, due to the complex influences of both substrates and contaminants, maintaining a clean and hydrophilic graphene surface is challenging. This, to be honest, severely hinders some advanced applications, and disturbs the fundamental research about the properties of graphene or its interactions with other materials. The high-quality CVD SLG shows advantages with its superior mechanical properties and thus can be used for flexible applications in energy fields. The semi-transparency of graphene endows the efficient modification of the substrate, providing extensive possibility for novel applications. Considering the applications of graphene in different areas, the wetting properties of aqueous droplets on graphene and related materials should be studied as well. What's more, miniaturization and integration of graphene-based energy devices is an irresistible trend to solve the future energy crisis. Meanwhile, the utilization of other layered materials, and their heterostructures should also be considered, given their advantages in tunable bandgap and work function.

Nomenclature

A	chemical vapor deposition	CVD
B	single layer graphene	SLG
C	water contact angle	WCA
D	molecular dynamics	MD
E	contact angle	CA
F	van der Waals	vdW
G	density functional	DF
H	polydimethylsiloxane	PDMS
I	environmental scanning electron microscope	ESEM
J	poly(methyl methacrylate)	PMMA
K	grain boundary	GB
L	Stone Wales	SW
M	single vacancy	SV
N	double vacancy	DV
O	bilayer graphene	BLG
P	multilayer graphene	MLG
Q	tri-layer graphene	TLG
R	vibrational sum-frequency-generation	VSFG
S	polyethylene terephthalate	PET

T	perovskite solar cells	PSCs
U	power-conversion efficiency	PCE
V	electrical double layer capacitors	EDLCs
W	electrical double layer	EDL
X	polyvinylidene fluoride	PVDF
Y	polytetrafluoroethylene	PTFE

6. Author Artwork

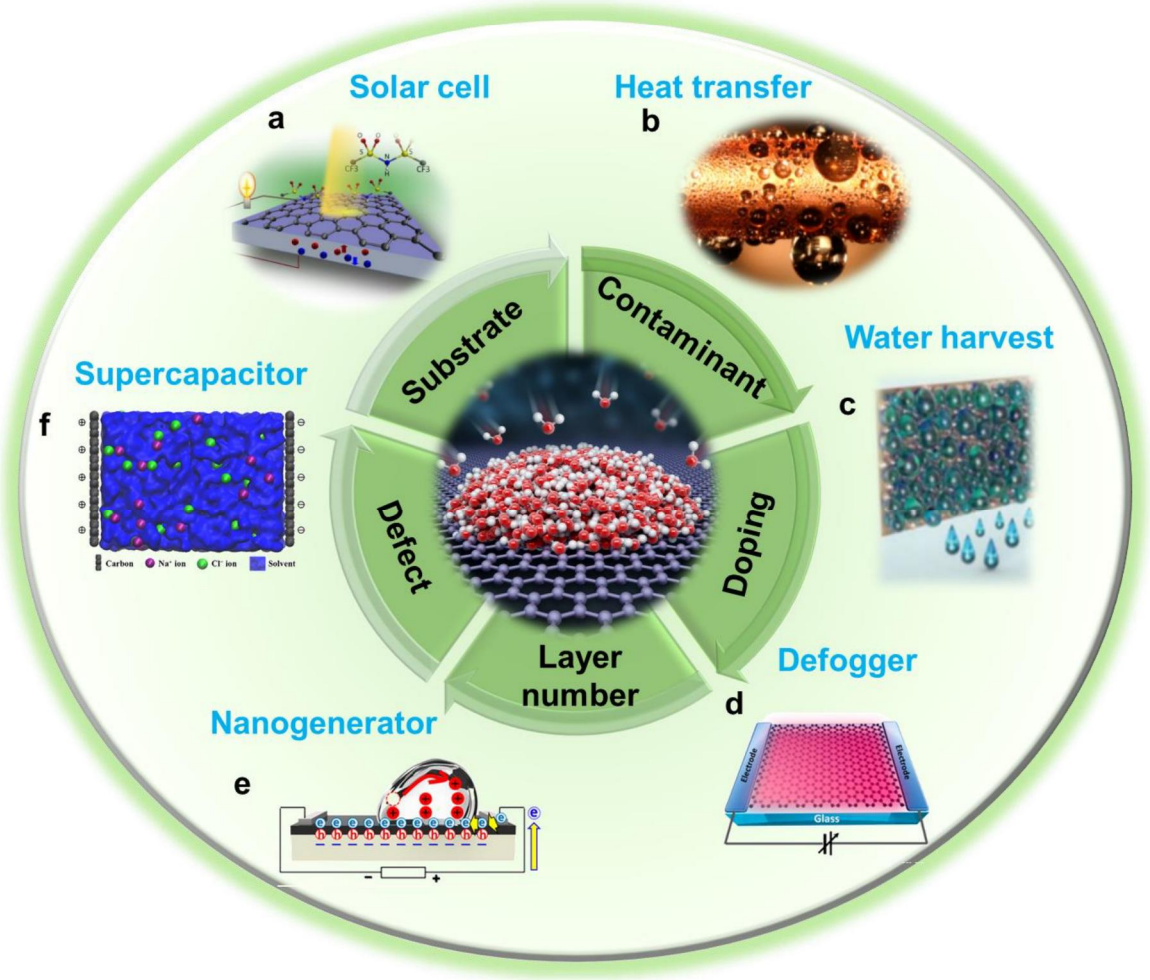

Figure 1. Scope of the review, which covers the origin of graphene wettability, discusses its influencing factors, and the application of graphene in water-involved energy applications. (a) Schematic of the SLG/n-Si Schottky junction solar cell. Reproduced with permission from [23]. Copyright 2012, American Chemical Society. (b) Water condensation on CVD SLG/Cu tubes. Reproduced with permission from [30]. Copyright 2015, American Chemical Society. (c) Schematic of the water condensation on hydrophobic SLG/Cu. Reproduced with permission from [32]. (d) Schematic of a directly grown graphene glass defogger. Reproduced with permission from [33]. Copyright 201, American Chemical Society. (e) Schematic of the SLG based tribo-voltaic nanogenerator. Reproduced with permission from [164]. Copyright 2016, American Chemistry Society. (f) Schematic showing the effect of graphene wettability on the electrolyte electro-sorption within graphene-based nonconfined and confined space. Reproduced with permission from [173]. Copyright 2019, ELSEVIER.

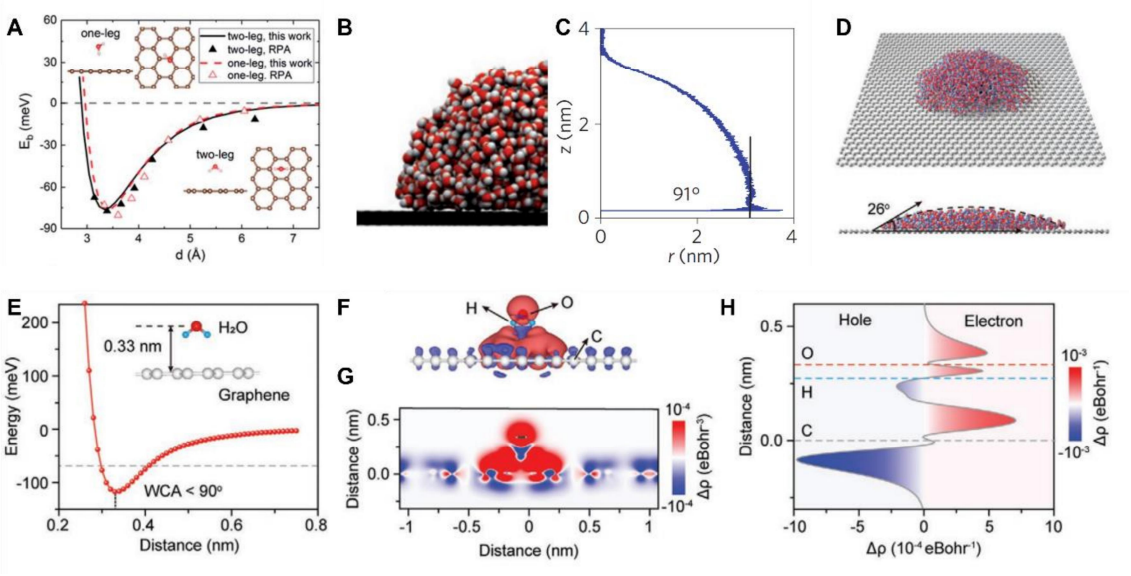

Figure 2. Interactions between water molecules and graphene. (a) Adsorption energy of water monomer on suspended graphene. Reproduced with permission of [45]. Copyright 2018, The Royal Society of Chemistry. (b) Post-equilibrium MD simulation snapshots of a water droplet lying on a flat-fixed suspended graphene. (c) Time average profile of the water droplet in (B) showing its shape, where r and z are droplet radius and height, respectively. Reproduced with permission from [48]. Copyright 2013, Nature Publishing. (d) MD simulation result showing the shape of a water nanodroplet on pristine graphene. (e) Adsorption energy of water monomer (two-leg configuration) as a function of the distance from O atom in water to graphene plane. (f, g) First-principles simulations result of the charge transfer between water monomer and graphene, where red and blue clouds correspond to the accumulation and depletion of electrons, respectively. (h) Planar-averaged electron density difference as a function of the distance from O atom in water to the graphene plane. Reproduced with permission from [41]. Copyright 2021, Wiley-VCH.

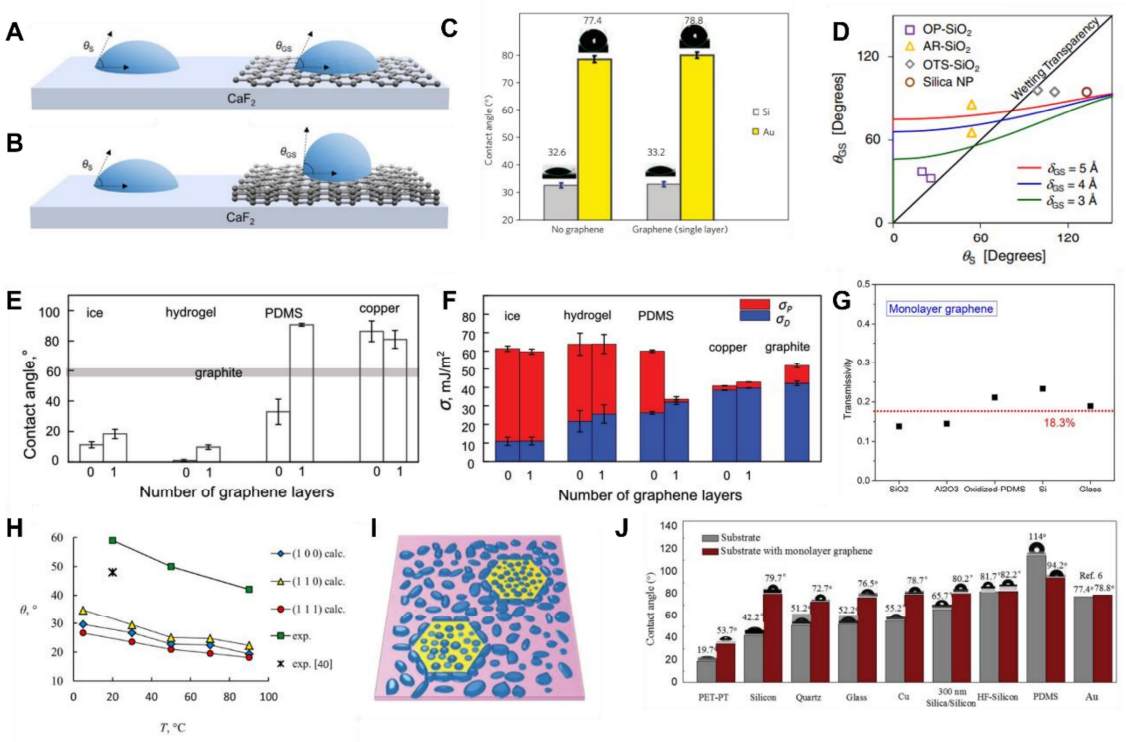

Figure 3. Wetting transparency of graphene. (a, b) Wettability of a bare CaF_2 substrate, SLG/CaF_2 and bilayer graphene (BLG)/CaF_2. Reproduced with permission from [174]. Copyright 2021, Elsevier. (c) WCAs on Si and glass without and with SLG coating. Reproduced with permission from [52]. Copyright 2012, Nature Publishing. (d) WCA of SLG supported by the solid substrate (θ_{GS}) as a function of the WCA of the bare substrate (θ_S), with different equilibrium contact separations between graphene and the solid (δ_{GS}). Reproduced with permission from [53]. Copyright 2012, American Physical Society. (e) WCAs of ice, hydrogel, PDMS and Cu without and with SLG coating. (f) Calculated polar and dispersive components of the surface energy of graphene-covered substrates *versus* the bare substrates. Reproduced with permission from [42]. Copyright 2018, Wiley-VCH. (g) Polar transmittance of SLG to different substrates. Reproduced with permission from [55]. Copyright 2018, Elsevier. (h) Impact of Cu crystal planes and temperature on wettability of SLG/Cu. Reproduced with permission from [61]. Copyright 2023, Elsevier. (i) Schematic showing the mechanism of the optical visualization of graphene on substrates. (j) WCA of various substrates with and without SLG coating. Reproduced with permission from [68]. Copyright 2016, Wiley-VCH.

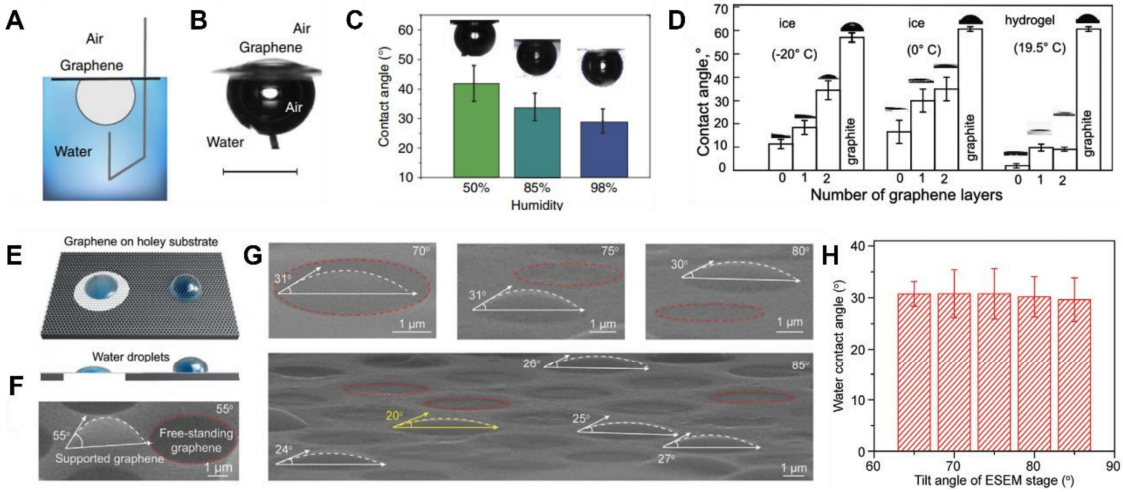

Figure 4. Measurement of intrinsic wettability in pristine graphene. (a) Schematic showing the captive bubble setup for WCA measurement of free-standing graphene. (b) Photograph of graphene on top of an air bubble (side view). Scale bar: 2 mm. (c) WCA of free-standing SLG measured in different humidity. Reproduced with permission from [43]. Copyright 2018, Nature Publishing. (d) WCA of SLG and BLG on ice and hydrogel. Reproduced with permission from [42]. Copyright 2018, Wiley-VCH. (e) Schematic showing the intrinsic hydrophilicity of pristine graphene excluding the impact of underlying substrate. (f) ESEM image showing the water droplet on supported SLG. (g) ESEM images showing the water droplets on suspended graphene acquired at different tilt angles. (h) Statistics of the WCA measured at different tilt angles. Reproduced with permission from [41]. Copyright 2022, Wiley-VCH.

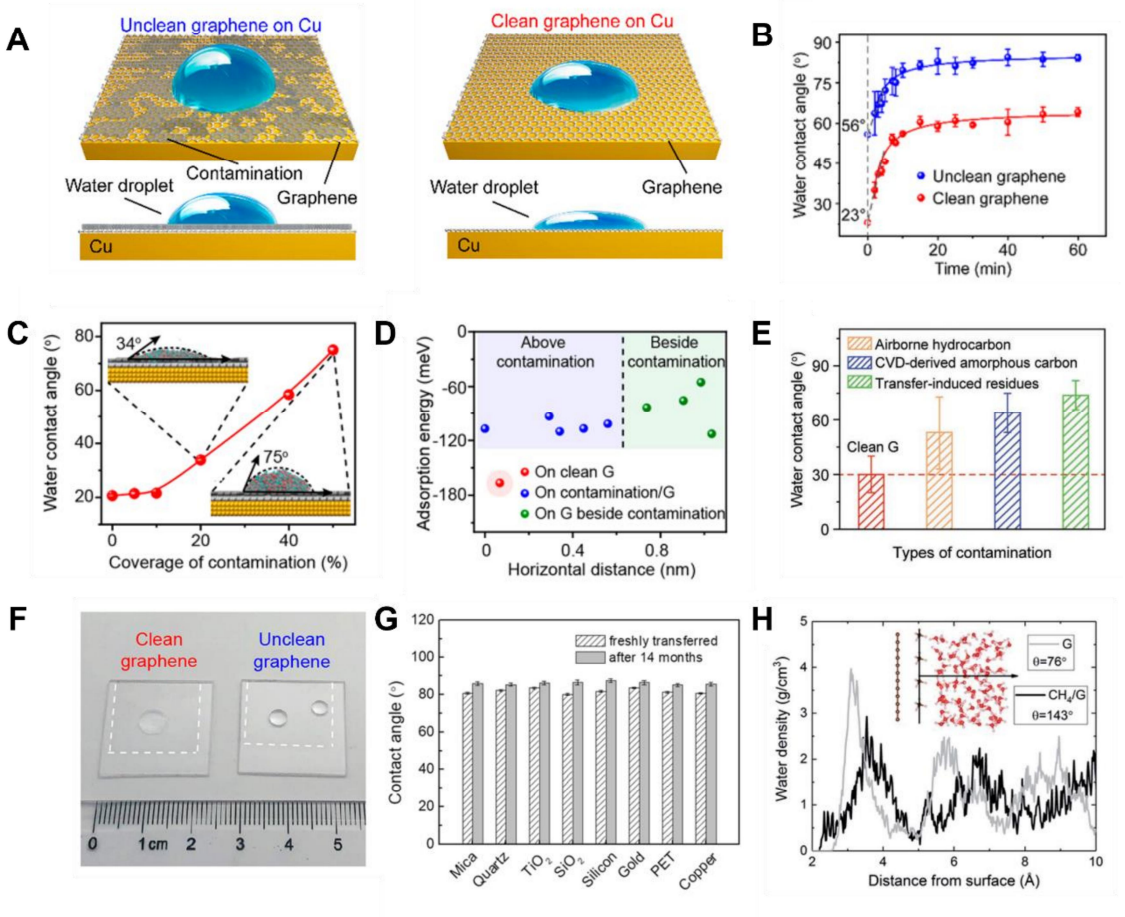

Figure 5. Impact of surface contamination on graphene wettability. (a) Schematic showing the effect of surface contamination on SLG/Cu wettability. (b) Time evolution of the WCAs of the Cu-supported clean and unclean graphene after exposure in ambient air for 1 hour. (c) MD simulation results showing the relationship between the WCA of SLG/Cu and the coverage of amorphous carbon contamination. Inset: Side views of the water droplets on unclean graphene covered by contamination of 20% and 50% areal ratios. (d) Adsorption energy comparison of water molecules on clean and unclean graphene. Reproduced with permission from [64]. Copyright 2021, American Chemical Society. (e) WCA statistics of suspended clean graphene (red) and unclean graphene contaminated by airborne hydrocarbon (orange), CVD-derived amorphous carbon (blue), and transfer-induced residues (green). Reproduced with permission from [41]. Copyright 2022, Wiley-VCH. (f) Photograph of water droplets on clean (left) and unclean (right) graphene supported by quartz. Reproduced with permission from [64]. Copyright 2021, American Chemical Society. (g) WCAs of SLG-covered substrates before and after exposure to air for 14 months. Reproduced with permission from [63]. Copyright 2022, Wiley-VCH. (h) Water density profile of graphene with and without hydrocarbon (CH_4) contamination. Reproduced with permission from [45]. Copyright 2018, The Royal Society of Chemistry.

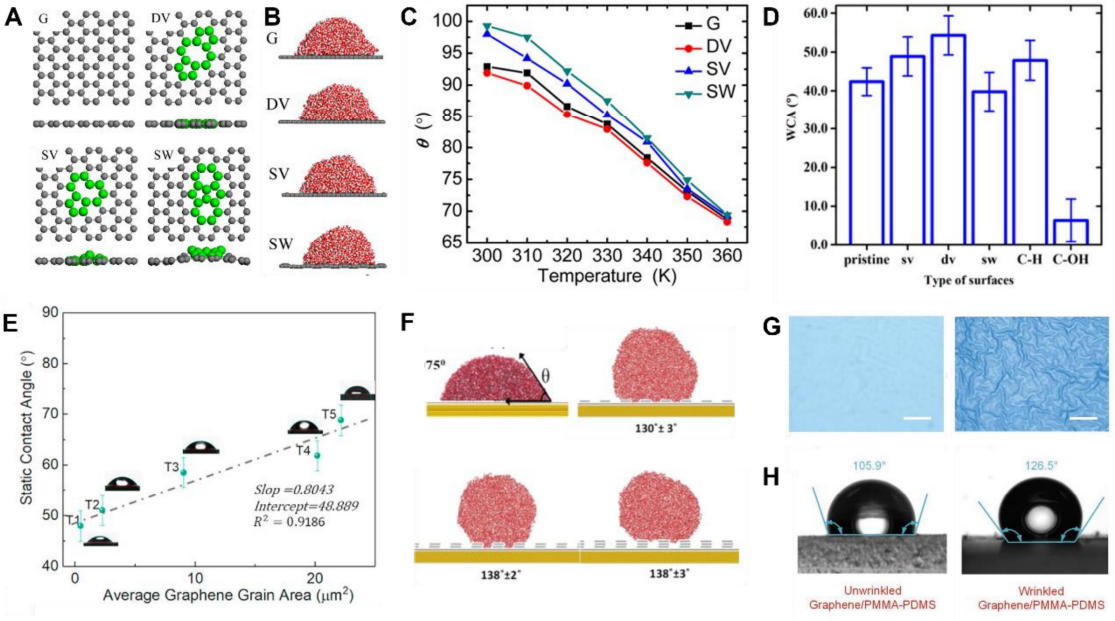

Figure 6. Impact of defects on graphene wettability. (a) Structures of perfect and defective graphene. (b) Snapshots of the water droplets on different types of graphene. (c) MD simulation results of WCA of different types of graphene as a function of temperature. Reproduced with permission from [84]. Copyright 2017, American Chemical Society. (d) MD simulation results of WCAs of pristine graphite, graphite with SV, DV, and SW defects, graphite with SV defects and hydrogen chemisorption (C-H) and graphite with SV defects and hydroxyl chemisorption (C-OH). Reproduced with permission from [85]. Copyright 2014, American Chemical Society. (e) Static WCA of graphene with different grain sizes. Reproduced with permission from [88]. Copyright 2018, Elsevier. (f) MD simulation results showing impact of roughness-induced chemical heterogeneity on graphene wettability. (g) OM image of the unwrinkled and WG/PMMA-PDMS surface. (h) WCA of the unwrinkled graphene/PMMA-PDMS and WG/PMMA-PDMS. Reproduced with permission from [96]. Copyright 2020, Wiley-VCH.

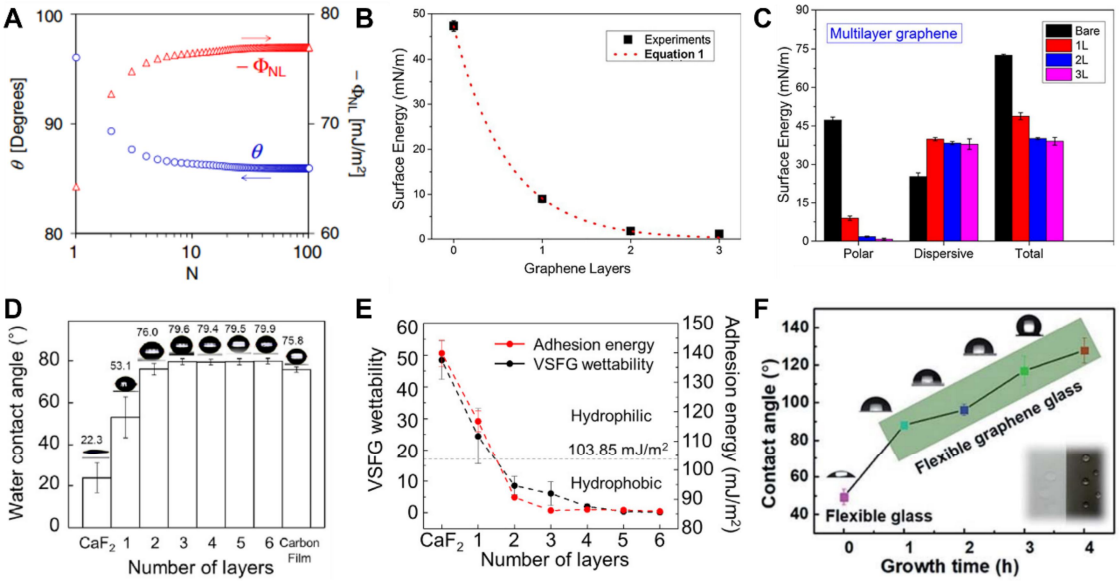

Figure 7. Impact of layer number on graphene wettability. (a) Calculated WCAs (θ) and the total vdW interaction potential per unit area between water and a contacting graphene ($-\Phi_{NL}$) as a function of the graphene layer number (N). Reproduced with permission from [53]. Copyright 2012, American Physical Society. (b) Polar surface energy of glass with the increase of graphene layer number. Reproduced with permission from [45]. Copyright 2018, The Royal Society of Chemistry. (c) Polar, dispersive, and total surface energy of bare glass, SLG/glass, BLG/glass, and TLG/glass. (d) WCAs of CaF_2 without and with graphene coating. (e) The vibrational sum-frequency-generation (VSFG) wettability and water adhesion energy of CaF_2 without and with graphene coating. Reproduced with permission from [102]. Copyright 2022, Elsevier. (f) WCA dependence on the growth time of graphene/glass. Inset: Photograph of the water droplets on glass (left) and graphene/glass (right). Reproduced with permission from [105]. Copyright 2022, American Chemical Society.

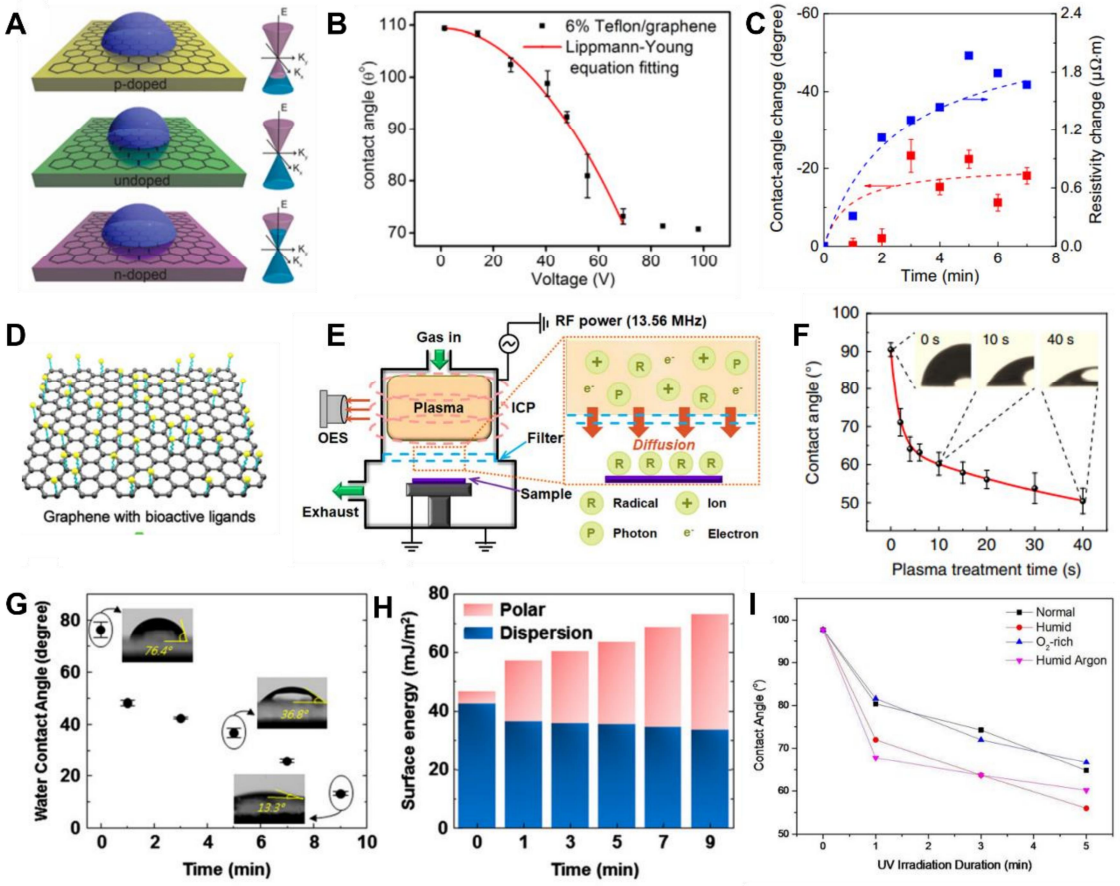

Figure 8. Impact of doping on graphene wettability. (a) Schematic showing the different wetting states of pristine and doped graphene. Reproduced with permission from [106]. Copyright 2016, American Chemical Society. (b) Impact of applied gate voltage on graphene wettability. Reproduced with permission from [110]. Copyright 2012, IOP Publishing. (c) WCA and resistivity change of graphene as a function of the functionalization time using Chop pyrene derivative. Reproduced with permission from [119]. Copy 2017, Wiley-VCH. (d) Schematic of the covalent functionalized SLG using bioactive ligands. Reproduced with permission from [117]. Copyright 2019, American Chemical Society. (e) Schematic of the plasma treatment of SLG for surface modification. Reproduced with permission from [175]. Copyright 2019, IOP Publishing. (f) WCA of graphene as a function of O_2 plasma treatment time. Reproduced with permission from [69]. Copyright 2020, Nature Publishing. (g) WCA of graphene/glass as a function of ozone treatment time. (h) The dependence of polar and dispersive components in the surface energy of graphene on the ozone treatment time. Reproduced with permission from [128]. Copyright 2013, Elsevier. (i) Impact of atmosphere on the wettability regulation of graphene after ozone treatment. Reproduced with permission from [76]. Copyright 2014, Nature Publishing.

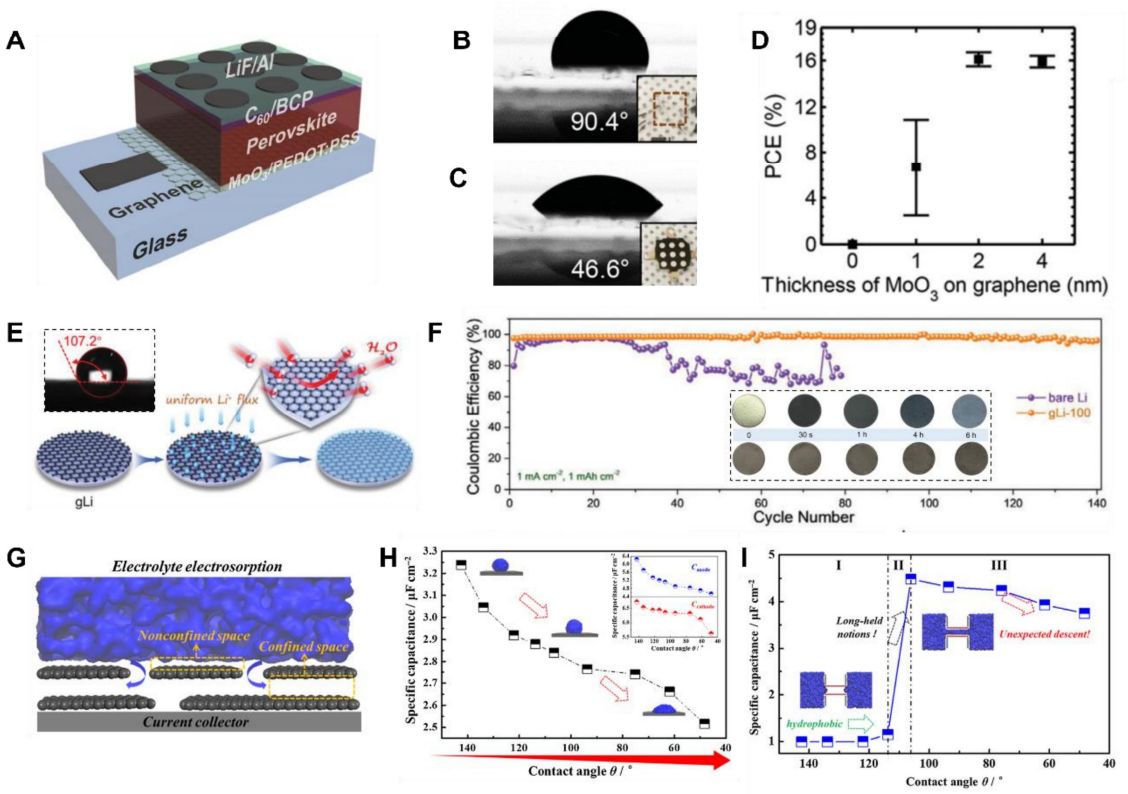

Figure 9. Impact of graphene wettability in solar cell, battery, and supercapacitor applications. (a) Schematic of the inverted PSCs using graphene as a transparent anode. (b, c) WCAs of SLG/glass (b) and MoO_3 (1 nm)/SLG/glass (c). (d) Relationship between average power conversion efficiency (PCE) and the thickness of MoO_3 on graphene. Reproduced with permission from [24]. Copyright 2016, Wiley-VCH. (E) Schematic showing the function of graphene in inhibiting the formation of Li dendrite and preventing the moisture attack. Inset: WCA of graphene-coated Li electrode (g-Li). (f) Coulombic efficiency in half-cells for g-Li and bare Li. Inset: Serial photographs of the bare-Li and graphene-coated Li anodes after exposure to air for 6 hours. Reproduced with permission from [25]. Copyright 2021, Wiley-VCH. (g) Schematic showing the effect of graphene wettability on the electrolyte electro-sorption within graphene-based nonconfined and confined spaces. (h, i) Capacitive results for nonconfined (h) and confined (i) space. Reproduced with permission from[27]. Copyright 2019, ELSEVIER.

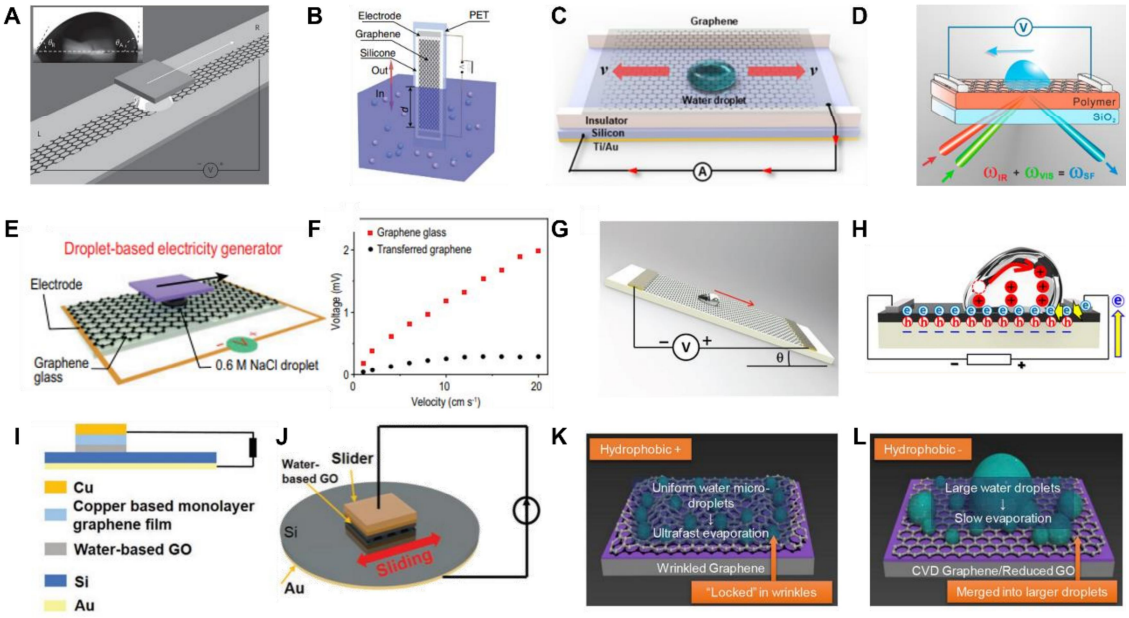

Figure 10. CVD graphene-based nanogenerator and the effect of graphene wettability. (a) Schematic showing the electricity generation while placing a SiO_2/Si wafer on top of a water droplet on SLG surface. Reproduced with permission from [28]. Copyright 2014, Nature Publishing. (b) Schematic showing the moving of graphene sample on a PET substrate vertically across the water surface. Reproduced with permission from [159]. Copyright 2014, Nature Publishing. (c) Schematic of the DC electricity generation in the graphene-water-Si structure. Reproduced with permission from [161]. Copyright 2021, American Chemistry Society. (d) Experimental setup for electricity generation on a device consisting of a graphene/polymer film on a SiO2 plate. Reproduced with permission from [7]. Copyright 2018, American Chemistry Society. (e) Schematic of the water droplet-based hydro-voltaic electricity generator using directly grown graphene/glass. (f) Comparison of the voltage signals produced by dragging a droplet on directly grown graphene and transferred graphene. Reproduced with permission from [163]. Copyright 2022, Oxford Academic. (g) Schematic of measurement of the electrical response to the flow of a certain volume of water over graphene-PVDF heterostructure which is fixed on a slope. Reproduced with permission from [176]. Copyright 2017, Wiley-VCH. (h) Schematic of charge distribution during the water droplet movement over the surface of the graphene on PTFE. Reproduced with permission from [164]. Copyright 2016, American Chemistry Society. (i) The structure and circuit connection of the graphene-based tribovoltaic nanogenerator. (i) A 3D schematic and external circuit of interfacial lubrication tribovoltaic nanogenerator. Reproduced with permission from [29]. Copyright 2022, Wiley-VCH. (k,l) Schematic showing the water condensation on hydrophobic WG and less hydrophobic unwrinkled graphene surface. Reproduced with permission from [97]. Copyright 2019, ELSEVIER.

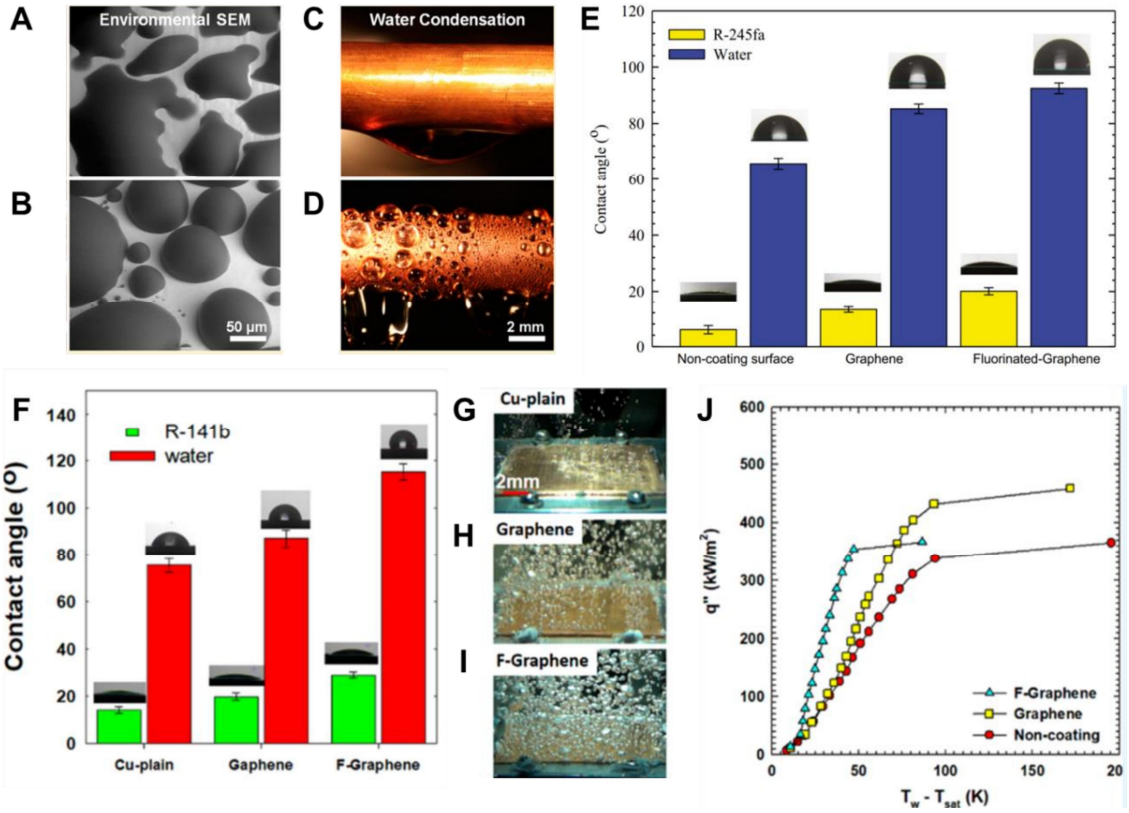

Figure 11. Enhanced heat transfer with the participation of hydrophobic CVD graphene. (a, b) ESEM images of water droplets on bare Cu and CVD SLG/Cu surfaces. (c, d) Photograph of water condensation on bare Cu (c) and SLG/Cu tubes (d). Reproduced with permission from [30]. Copyright 2015, American Chemical Society. (e) CA of water (blue) and R-245fa (yellow) on non-coating surface, SLG and fluorinated graphene. Reproduced with permission from [165]. Copyright 2022, The Author(s), under exclusive license to Springer-Verlag GmbH Germany, part of Springer Nature 2022. (f) CA of water (red) and R-141b (green) on Cu, SLG/Cu and functionalized-SLG (F-SLG)/Cu. (g-i) Boiling visualization on Cu-plain, SLG/Cu and F-SLG/Cu. (j) Boiling curves on the three types of surfaces mentioned in (f-i). Reproduced with permission from [31]. Copyright 2020, American Chemical Society.

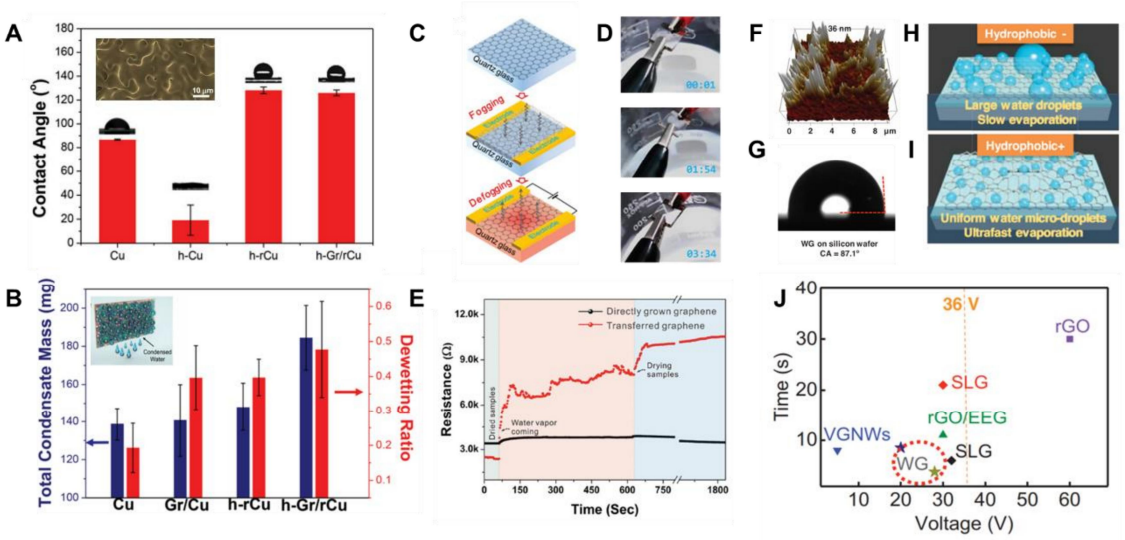

Figure 12. Water harvest and defogging using CVD graphene with tunable wettability. (a) WCA of different Cu substrates with and without graphene coating. Inset: OM image of the electroplated and thermal annealed Cu after graphene growth. (b) Total condensation mass and dewetting ratio for the four types of surfaces. Inset: Water harvesting by the corrosion resistant hydrophobic copper surface. Reproduced with permission from [32]. Copyright 2014, Wiley-VCH. (c) Schematic of the fogging and defogging process. (d) Photograph of the defogging process at a bias of 20 V. Reproduced with permission from [170]. Copyright 2017, Wiley-VCH. (e) The resistance profiles of directly grown graphene defogger and transferred graphene defogger before and after exposure to fog. Reproduced with permission from [169]. Copyright 2015, Wiley-VCH. (f) AFM image of the WG. (g) WCA of the WG on Si wafer. (h, i) Schematic showing the influence of graphene wettability on water evaporation. (J) Performance comparison of differing graphene-based defoggers. Reproduced with permission from [34]. Copyright 2020, Wiley-VCH.

Acknowledgements

This work was supported by the National Natural Science Foundation of China (No. 11904389) and GHfund B (No. 202202022704).

All authors listed have made a substantial, direct, and intellectual contribution to the work, and approved it for publication.

References

[1] Y. Li, Y. Zhang, J. Zhang, Z. Xiang, Z. Li, Research on the influencing factors of clean heating compound transformation under the carbon neutrality goal, Frontiers in Environmental Science, 10 (2022).

[2] L. Riboldi, E.F. Alves, M. Pilarczyk, E. Tedeschi, L.O. Nord, Optimal Design of a Hybrid Energy System for the Supply of Clean and Stable Energy to Offshore Installations, Frontiers in Energy Research, 8 (2020).

[3] Z. Xia, Z. Xiang, Editorial: Catalysts for Clean Energy Conversion and Storage, Frontiers in Materials, 7 (2020).

[4] S. Ramachandran, M. Rupakheti, R. Cherian, M.G. Lawrence, Climate Benefits of Cleaner Energy Transitions in East and South Asia Through Black Carbon Reduction, Frontiers in Environmental Science, 10 (2022).

[5] H. Lu, W. Shi, Y. Guo, W. Guan, C. Lei, G. Yu, Materials Engineering for Atmospheric Water Harvesting: Progress and Perspectives, Adv Mater, 34 (2022) e2110079.

[6] X. Wang, F. Lin, X. Wang, S. Fang, J. Tan, W. Chu, R. Rong, J. Yin, Z. Zhang, Y. Liu, W. Guo, Hydrovoltaic technology: from mechanism to applications, Chem Soc Rev, 51 (2022) 4902-4927.

[7] S. Yang, Y. Su, Y. Xu, Q. Wu, Y. Zhang, M.B. Raschke, M. Ren, Y. Chen, J. Wang, W. Guo, Y. Ron Shen, C. Tian, Mechanism of Electric Power Generation from Ionic Droplet Motion on Polymer Supported Graphene, J Am Chem Soc, 140 (2018) 13746-13752.

[8] J. Tan, X. Wang, W. Chu, S. Fang, C. Zheng, M. Xue, X. Wang, T. Hu, W. Guo, Harvesting Energy from Atmospheric Water: Grand Challenges in Continuous Electricity Generation, Adv Mater, (2023) e2211165.

[9] J. Yin, J. Zhou, S. Fang, W. Guo, Hydrovoltaic Energy on the Way, Joule, 4 (2020) 1852-1855.

[10] Z. Zhang, X. Li, J. Yin, Y. Xu, W. Fei, M. Xue, Q. Wang, J. Zhou, W. Guo, Emerging hydrovoltaic technology, Nat Nanotechnol, 13 (2018) 1109-1119.

[11] S.J. Lee, J. Theerthagiri, P. Nithyadharseni, P. Arunachalam, D. Balaji, A. Madan Kumar, J. Madhavan, V. Mittal, M.Y. Choi, Heteroatom-doped graphene-based materials for sustainable energy applications: A review, Renewable and Sustainable Energy Reviews, 143 (2021).

[12] X. Li, Y. Wang, Y. Zhao, J. Zhang, L. Qu, Graphene Materials for Miniaturized Energy Harvest and Storage Devices, Small Structures, 3 (2021).

[13] X. Zhao, J. E, G. Wu, Y. Deng, D. Han, B. Zhang, Z. Zhang, A review of studies using graphenes in energy conversion, energy storage and heat transfer development, Energy Conversion and Management, 184 (2019) 581-599.

[14] J.P.G. Tarelho, M.P. Soares dos Santos, J.A.F. Ferreira, A. Ramos, S. Kopyl, S.O. Kim, S. Hong, A. Kholkin, Graphene-based materials and structures for energy harvesting with fluids – A review, Materials Today, 21 (2018) 1019-1041.

[15] H. Chen, J. Zhang, X. Liu, Z. Liu, Effect of Gas-Phase Reaction on the CVD Growth of Graphene, Acta Physico Chimica Sinica, 0 (2021) 2101053-2101050.

[16] K. Jia, Z. Ma, W. Wang, Y. Wen, H. Li, Y. Zhu, J. Yang, Y. Song, J. Shao, X. Liu, Toward batch synthesis of high-quality graphene by cold-wall chemical vapor deposition approach, Nano Research, 15 (2022) 9683-9688.

[17] L. Lin, B. Deng, J. Sun, H. Peng, Z. Liu, Bridging the gap between reality and ideal in chemical vapor deposition growth of graphene, Chemical reviews, 118 (2018) 9281-9343.

[18] X. Liu, J. Zhang, H. Chen, Z. Liu, Synthesis of Superclean Graphene, Acta Physico Chimica Sinica, 0 (2021) 2012047-2012040.

[19] J. Zhang, L. Sun, K. Jia, X. Liu, T. Cheng, H. Peng, L. Lin, Z. Liu, New Growth Frontier: Superclean Graphene, ACS Nano, 14 (2020) 10796-10803.

[20] L. Lin, J. Zhang, H. Su, J. Li, L. Sun, Z. Wang, F. Xu, C. Liu, S. Lopatin, Y. Zhu, K. Jia, S. Chen, D. Rui, J. Sun, R. Xue, P. Gao, N. Kang, Y. Han, H.Q. Xu, Y. Cao, K.S. Novoselov, Z. Tian, B. Ren, H. Peng, Z. Liu, Towards super-clean graphene, Nat Commun, 10 (2019) 1912.

[21] A. Khan, M.R. Habib, R.R. Kumar, S.M. Islam, V. Arivazhagan, M. Salman, D. Yang, X. Yu, Wetting behaviors and applications of metal-catalyzed CVD grown graphene, Journal of Materials Chemistry A, 6 (2018) 22437-22464.

[22] J. Feng, Z. Guo, Wettability of graphene: from influencing factors and reversible conversions to potential applications, Nanoscale Horiz, 4 (2019) 339-364.

[23] X. Miao, S. Tongay, M.K. Petterson, K. Berke, A.G. Rinzler, B.R. Appleton, A.F. Hebard, High efficiency graphene solar cells by chemical doping, Nano Lett, 12 (2012) 2745-2750.

[24] H. Sung, N. Ahn, M.S. Jang, J.-K. Lee, H. Yoon, N.-G. Park, M. Choi, Transparent Conductive Oxide-Free Graphene-Based Perovskite Solar Cells with over 17% Efficiency, Advanced Energy Materials, 6 (2016).

[25] Y. Ma, P. Qi, J. Ma, L. Wei, L. Zhao, J. Cheng, Y. Su, Y. Gu, Y. Lian, Y. Peng, Y. Shen, L. Chen, Z. Deng, Z. Liu, Wax-Transferred Hydrophobic CVD Graphene Enables Water-Resistant and Dendrite-Free Lithium Anode toward Long Cycle Li-Air Battery, Adv Sci (Weinh), 8 (2021) e2100488.

[26] G. Jeanmairet, B. Rotenberg, D. Borgis, M. Salanne, Study of a water-graphene capacitor with molecular density functional theory, J Chem Phys, 151 (2019) 124111.

[27] H. Yang, Z. Bo, J. Yan, K. Cen, Influence of wettability on the electrolyte electrosorption within graphene-like nonconfined and confined space, International Journal of Heat and Mass Transfer, 133 (2019) 416-425.

[28] J. Yin, X. Li, J. Yu, Z. Zhang, J. Zhou, W. Guo, Generating electricity by moving a droplet of ionic liquid along graphene, Nat Nanotechnol, 9 (2014) 378-383.

[29] W. Qiao, Z. Zhao, L. Zhou, D. Liu, S. Li, P. Yang, X. Li, J. Liu, J. Wang, Z.L. Wang, Simultaneously Enhancing Direct - Current Density and Lifetime of Tribovotaic Nanogenerator via Interface Lubrication, Advanced Functional Materials, 32 (2022).

[30] D.J. Preston, D.L. Mafra, N. Miljkovic, J. Kong, E.N. Wang, Scalable graphene coatings for enhanced condensation heat transfer, Nano Lett, 15 (2015) 2902-2909.

[31] C.Y. Su, C.Y. Yang, B.W. Jhang, Y.L. Hsieh, Y.Y. Sin, C.C. Huang, Pool Boiling Heat Transfer Enhanced by Fluorinated Graphene as Atomic Layered Modifiers, ACS Appl Mater Interfaces, 12 (2020) 10233-10239.

[32] G.T. Kim, S.J. Gim, S.M. Cho, N. Koratkar, I.K. Oh, Wetting-transparent graphene films for hydrophobic water-harvesting surfaces, Adv Mater, 26 (2014) 5166-5172.

[33] J. Sun, Y. Chen, M.K. Priydarshi, Z. Chen, A. Bachmatiuk, Z. Zou, Z. Chen, X. Song, Y. Gao, M.H. Rummeli, Y. Zhang, Z. Liu, Direct Chemical Vapor Deposition-Derived Graphene Glasses Targeting Wide Ranged Applications, Nano Lett, 15 (2015) 5846-5854.

[34] Z. Li, Z. Zhen, M. Chai, X. Zhao, Y. Zhong, H. Zhu, Transparent Electrothermal Film Defoggers and Antiicing Coatings based on Wrinkled Graphene, Small, 16 (2020) e1905945.

[35] W. Zhao, Y. Jiang, W. Yu, Z. Yu, X. Liu, Wettability Controlled Surface for Energy Conversion, Small, 18 (2022) e2202906.

[36] Y. Wan, Y. Gao, J. Wang, Y. Yang, Z. Xia, Rapid Water Harvesting and Nonthermal Drying in Humid Air by N-Doped Graphene Micropads, Langmuir, 35 (2019) 12389-12399.

[37] D. Parobek, H. Liu, Wettability of graphene, 2D Materials, 2 (2015).

[38] L.A. Belyaeva, G.F. Schneider, Wettability of graphene, Surface Science Reports, 75 (2020).

[39] P. Snapp, J.M. Kim, C. Cho, J. Leem, M.F. Haque, S. Nam, Interaction of 2D materials with liquids: wettability, electrochemical properties, friction, and emerging directions, NPG Asia Materials, 12 (2020).

[40] C. Melios, C.E. Giusca, V. Panchal, O. Kazakova, Water on graphene: review of recent progress, 2D Materials, 5 (2018).

[41] J. Zhang, K. Jia, Y. Huang, X. Liu, Q. Xu, W. Wang, R. Zhang, B. Liu, L. Zheng, H. Chen, P. Gao, S. Meng, L. Lin, H. Peng, Z. Liu, Intrinsic Wettability in Pristine Graphene, Adv Mater, 34 (2022) e2103620.

[42] L.A. Belyaeva, P.M.G. van Deursen, K.I. Barbetsea, G.F. Schneider, Hydrophilicity of Graphene in Water through Transparency to Polar and Dispersive Interactions, Adv Mater, 30 (2018).

[43] A.V. Prydatko, L.A. Belyaeva, L. Jiang, L.M.C. Lima, G.F. Schneider, Contact angle measurement of free-standing square-millimeter single-layer graphene, Nat Commun, 9 (2018) 4185.

[44] T. Werder, J.H. Walther, R. Jaffe, T. Halicioglu, P. Koumoutsakos, On the water− carbon interaction for use in molecular dynamics simulations of graphite and carbon nanotubes, The Journal of Physical Chemistry B, 107 (2003) 1345-1352.

[45] J. Liu, C.-Y. Lai, Y.-Y. Zhang, M. Chiesa, S.T. Pantelides, Water wettability of graphene: interplay between the interfacial water structure and the electronic structure, RSC Advances, 8 (2018) 16918-16926.

[46] J. Ma, A. Michaelides, D. Alfè, L. Schimka, G. Kresse, E. Wang, Adsorption and diffusion of water on graphene from first principles, Physical Review B, 84 (2011).

[47] S. Khan, J.K. Singh, Wetting transition of nanodroplets of water on textured surfaces: a molecular dynamics study, Molecular Simulation, 40 (2013) 458-468.

[48] C.J. Shih, M.S. Strano, D. Blankschtein, Wetting translucency of graphene, Nat Mater, 12 (2013) 866-869.

[49] I. Hamada, Adsorption of water on graphene: A van der Waals density functional study, Physical Review B, 86 (2012).

[50] R.P. Misra, D. Blankschtein, Insights on the Role of Many-Body Polarization Effects in the Wetting of Graphitic Surfaces by Water, The Journal of Physical Chemistry C, 121 (2017) 28166-28179.

[51] A. Kozbial, Z. Li, C. Conaway, R. McGinley, S. Dhingra, V. Vahdat, F. Zhou, B. D'Urso, H. Liu, L. Li, Study on the surface energy of graphene by contact angle measurements, Langmuir, 30 (2014) 8598-8606.

[52] J. Rafiee, X. Mi, H. Gullapalli, A.V. Thomas, F. Yavari, Y. Shi, P.M. Ajayan, N.A. Koratkar, Wetting transparency of graphene, Nat Mater, 11 (2012) 217-222.

[53] C.J. Shih, Q.H. Wang, S. Lin, K.C. Park, Z. Jin, M.S. Strano, D. Blankschtein, Breakdown in the wetting transparency of graphene, Phys Rev Lett, 109 (2012) 176101.

[54] L.A. Belyaeva, P.M. van Deursen, K.I. Barbetsea, G.F. Schneider, Hydrophilicity of graphene in water through transparency to polar and dispersive interactions, Advanced materials, 30 (2018) 1703274.

[55] F. Du, J. Huang, H. Duan, C. Xiong, J. Wang, Wetting transparency of supported graphene is regulated by polarities of liquids and substrates, Applied Surface Science, 454 (2018) 249-255.

[56] D. Kim, N.M. Pugno, M.J. Buehler, S. Ryu, Solving the Controversy on the Wetting Transparency of Graphene, Sci Rep, 5 (2015) 15526.

[57] Y. Zhao, G. Wang, W. Huang, X. Fan, Y. Deng, J. Zhang, T. Wei, R. Duan, J. Wang, L. Sun, Investigations on the wettability of graphene on a micron-scale hole array substrate, RSC Advances, 6 (2016) 1999-2003.

[58] T. Ondarcuhu, V. Thomas, M. Nunez, E. Dujardin, A. Rahman, C.T. Black, A. Checco, Wettability of partially suspended graphene, Sci Rep, 6 (2016) 24237.

[59] Z. Zheng, Y. Liu, Y. Bai, J. Zhang, Z. Han, L. Ren, Fabrication of biomimetic hydrophobic patterned graphene surface with ecofriendly anti-corrosion properties for Al alloy, Colloids and Surfaces A: Physicochemical and Engineering Aspects, 500 (2016) 64-71.

[60] Y. Song, Y. Liu, H. Jiang, Y. Zhang, Z. Han, L. Ren, Biomimetic super hydrophobic structured graphene on stainless steel surface by laser processing and transfer technology, Surface and Coatings Technology, 328 (2017) 152-160.

[61] S.Y. Misyura, V.A. Andryushchenko, D.V. Smovzh, V.S. Morozov, Experimental data and modeling of wettability on graphene-coated copper, Materials Science and Engineering: B, 277 (2022).

[62] L.A. Belyaeva, C. Tang, L. Juurlink, G.F. Schneider, Macroscopic and Microscopic Wettability of Graphene, Langmuir, 37 (2021) 4049-4055.

[63] X. Li, Z. Li, Y. Long, Y. He, B. Li, J. Li, H. Qiu, J. Yin, W. Guo, Wetting Stability of Supported Graphene in Ambient Environment, Advanced Engineering Materials, 24 (2022).

[64] J. Zhang, K. Jia, Y. Huang, Y. Wang, N. Liu, Y. Chen, X. Liu, X. Liu, Y. Zhu, L. Zheng, H. Chen, F. Liang, M. Zhang, X. Duan, H. Wang, L. Lin, H. Peng, Z. Liu, Hydrophilic, Clean Graphene for Cell Culture and Cryo-EM Imaging, Nano Lett, 21 (2021) 9587-9593.

[65] S.Y. Misyura, V.S. Morozov, D.V. Smovzh, V.G. Makotchenko, D.V. Feoktistov, E.G. Orlova, A.G. Islamova, M.N. Khomyakov, O.A. Solnyshkina, Wetting properties of graphene and multilayer graphene deposited on copper: The influence of copper topography, Thin Solid Films, 755 (2022).

[66] S.Y. Misyura, V.A. Andryushchenko, V.S. Morozov, The effect of temperature on the contact angle of a water drop on graphene and graphene synthesized on copper, Materials Science and Engineering: B, 290 (2023).

[67] R. Raj, S.C. Maroo, E.N. Wang, Wettability of graphene, Nano Lett, 13 (2013) 1509-1515.

[68] K. Xia, M. Jian, W. Zhang, Y. Zhang, Visualization of Graphene on Various Substrates Based on Water Wetting Behavior, Advanced Materials Interfaces, 3 (2016).

[69] L. Zheng, Y. Chen, N. Li, J. Zhang, N. Liu, J. Liu, W. Dang, B. Deng, Y. Li, X. Gao, C. Tan, Z. Yang, S. Xu, M. Wang, H. Yang, L. Sun, Y. Cui, X. Wei, P. Gao, H.W. Wang, H. Peng, Robust ultraclean atomically thin membranes for atomic-resolution electron microscopy, Nat Commun, 11 (2020) 541.

[70] Z. Li, A. Kozbial, N. Nioradze, D. Parobek, G.J. Shenoy, M. Salim, S. Amemiya, L. Li, H. Liu, Water Protects Graphitic Surface from Airborne Hydrocarbon Contamination, ACS Nano, 10 (2016) 349-359.

[71] K. Jia, J. Zhang, L. Lin, Z. Li, J. Gao, L. Sun, R. Xue, J. Li, N. Kang, Z. Luo, M.H. Rummeli, H. Peng, Z. Liu, Copper-Containing Carbon Feedstock for Growing Superclean Graphene, J Am Chem Soc, 141 (2019) 7670-7674.

[72] J. Zhang, K. Jia, L. Lin, W. Zhao, H.T. Quang, L. Sun, T. Li, Z. Li, X. Liu, L. Zheng, R. Xue, J. Gao, Z. Luo, M.H. Rummeli, Q. Yuan, H. Peng, Z. Liu, Large-Area Synthesis of Superclean Graphene via Selective Etching of Amorphous Carbon with Carbon Dioxide, Angew Chem Int Ed Engl, 58 (2019) 14446-14451.

[73] Z. Li, Y. Wang, A. Kozbial, G. Shenoy, F. Zhou, R. McGinley, P. Ireland, B. Morganstein, A. Kunkel, S.P. Surwade, L. Li, H. Liu, Effect of airborne contaminants on the wettability of supported graphene and graphite, Nat Mater, 12 (2013) 925-931.

[74] A. Kozbial, Z. Li, J. Sun, X. Gong, F. Zhou, Y. Wang, H. Xu, H. Liu, L. Li, Understanding the intrinsic water wettability of graphite, Carbon, 74 (2014) 218-225.

[75] A. Kozbial, F. Zhou, Z. Li, H. Liu, L. Li, Are Graphitic Surfaces Hydrophobic?, Acc Chem Res, 49 (2016) 2765-2773.

[76] Z. Xu, Z. Ao, D. Chu, A. Younis, C.M. Li, S. Li, Reversible hydrophobic to hydrophilic transition in graphene via water splitting induced by UV irradiation, Sci Rep, 4 (2014) 6450.

[77] C. Mücksch, C. Rösch, C. Müller–Renno, C. Ziegler, H.M. Urbassek, Consequences of Hydrocarbon Contamination for Wettability and Protein Adsorption on Graphite Surfaces, The Journal of Physical Chemistry C, 119 (2015) 12496-12501.

[78] A.I. Aria, P.R. Kidambi, R.S. Weatherup, L. Xiao, J.A. Williams, S. Hofmann, Time Evolution of the Wettability of Supported Graphene under Ambient Air Exposure, J Phys Chem C Nanomater Interfaces, 120 (2016) 2215-2224.

[79] C.A. Amadei, C.Y. Lai, D. Heskes, M. Chiesa, Time dependent wettability of graphite upon ambient exposure: the role of water adsorption, J Chem Phys, 141 (2014) 084709.

[80] S.Y. Misyura, V.A. Andryushchenko, D.V. Smovzh, V.S. Morozov, Graphene wettability control: Texturing of the substrate and removal of airborne contaminants in the atmosphere of various gases, Journal of Molecular Liquids, 349 (2022).

[81] Y. Wu, N.R. Aluru, Graphitic carbon-water nonbonded interaction parameters, J Phys Chem B, 117 (2013) 8802-8813.

[82] J. Driskill, D. Vanzo, D. Bratko, A. Luzar, Wetting transparency of graphene in water, J Chem Phys, 141 (2014) 18C517.

[83] L. Liu, M. Qing, Y. Wang, S. Chen, Defects in graphene: generation, healing, and their effects on the properties of graphene: a review, Journal of Materials Science & Technology, 31 (2015) 599-606.

[84] X. Li, L. Li, Y. Wang, H. Li, X. Bian, Wetting and Interfacial Properties of Water on the Defective Graphene, The Journal of Physical Chemistry C, 117 (2013) 14106-14112.

[85] A. Ashraf, Y. Wu, M.C. Wang, N.R. Aluru, S.A. Dastgheib, S. Nam, Spectroscopic investigation of the wettability of multilayer graphene using highly ordered pyrolytic graphite as a model material, Langmuir, 30 (2014) 12827-12836.

[86] A. Kozbial, C. Trouba, H. Liu, L. Li, Characterization of the Intrinsic Water Wettability of Graphite Using Contact Angle Measurements: Effect of Defects on Static and Dynamic Contact Angles, Langmuir, 33 (2017) 959-967.

[87] M. Torabi Rad, M. Foroutan, Wettability of Penta-Graphene: A Molecular Dynamics Simulation Approach, The Journal of Physical Chemistry C, 126 (2022) 1590-1599.

[88] W. Chang, B. Peng, A.S. Khan, M. Alwazzan, Y. Zhang, X. Li, Y. Tong, C. Li, Grain size effects on the wettability of as-grown graphene and dropwise condensation, Carbon, 171 (2021) 507-513.

[89] C. Wang, Y. Liu, L. Lan, H. Tan, Graphene wrinkling: formation, evolution and collapse, Nanoscale, 5 (2013) 4454-4461.

[90] W. Zhu, T. Low, V. Perebeinos, A.A. Bol, Y. Zhu, H. Yan, J. Tersoff, P. Avouris, Structure and electronic transport in graphene wrinkles, Nano Lett, 12 (2012) 3431-3436.

[91] B. Deng, Z. Pang, S. Chen, X. Li, C. Meng, J. Li, M. Liu, J. Wu, Y. Qi, W. Dang, Wrinkle-free single-crystal graphene wafer grown on strain-engineered substrates, ACS nano, 11 (2017) 12337-12345.

[92] Y. Song, Y. Gao, X. Liu, J. Ma, B. Chen, Q. Xie, X. Gao, L. Zheng, Y. Zhang, Q. Ding, K. Jia, L. Sun, W. Wang, Z. Liu, B. Liu, P. Gao, H. Peng, T. Wei, L. Lin, Z. Liu, Transfer-Enabled Fabrication of Graphene Wrinkle Arrays for Epitaxial Growth of AlN Films, Adv Mater, 34 (2022) e2105851.

[93] N. Liu, Z. Pan, L. Fu, C. Zhang, B. Dai, Z. Liu, The origin of wrinkles on transferred graphene, Nano Research, 4 (2011) 996-1004.

[94] Z. Pan, N. Liu, L. Fu, Z. Liu, Wrinkle engineering: a new approach to massive graphene nanoribbon arrays, J Am Chem Soc, 133 (2011) 17578-17581.

[95] J.E. Andrews, Y. Wang, S. Sinha, P.W. Chung, S. Das, Roughness-Induced Chemical Heterogeneity Leads to Large Hydrophobicity in Wetting-Translucent Nanostructures, The Journal of Physical Chemistry C, 121 (2017) 10010-10017.

[96] K.M. Hu, Y.Q. Liu, L.W. Zhou, Z.Y. Xue, B. Peng, H. Yan, Z.F. Di, X.S. Jiang, G. Meng, W.M. Zhang, Delamination - Free Functional Graphene Surface by Multiscale, Conformal Wrinkling, Advanced Functional Materials, 30 (2020).

[97] Z. Zhen, Z. Li, X. Zhao, Y. Zhong, M. Huang, H. Zhu, A non-covalent cation-π interaction-based humidity-driven electric nanogenerator prepared with salt decorated wrinkled graphene, Nano Energy, 62 (2019) 189-196.

[98] M. Chiricotto, F. Martelli, G. Giunta, P. Carbone, Role of Long-Range Electrostatic Interactions and Local Topology of the Hydrogen Bond Network in the Wettability of Fully and Partially Wetted Single and Multilayer Graphene, The Journal of Physical Chemistry C, 125 (2021) 6367-6377.

[99] H. Wang, D. Orejon, D. Song, X. Zhang, G. McHale, H. Takamatsu, Y. Takata, K. Sefiane, Non-wetting of condensation-induced droplets on smooth monolayer suspended graphene with contact angle approaching 180 degrees, Communications Materials, 3 (2022).

[100] A. Rana, A. Patra, M. Annamalai, A. Srivastava, S. Ghosh, K. Stoerzinger, Y.L. Lee, S. Prakash, R.Y. Jueyuan, P.S. Goohpattader, N. Satyanarayana, K. Gopinadhan, M.M. Dykas, K. Poddar, S. Saha, T. Sarkar, B. Kumar, C.S. Bhatia, L. Giordano, Y. Shao-Horn, T. Venkatesan, Correlation of nanoscale behaviour of forces and macroscale surface wettability, Nanoscale, 8 (2016) 15597-15603.

[101] J.Y. Lu, T. Olukan, S.R. Tamalampudi, A. Al-Hagri, C.Y. Lai, M. Ali Al Mahri, H. Apostoleris, I. Almansouri, M. Chiesa, Insights into graphene wettability transparency by locally probing its surface free energy, Nanoscale, 11 (2019) 7944-7951.

[102] E. Kim, D. Kim, K. Kwak, Y. Nagata, M. Bonn, M. Cho, Wettability of graphene, water contact angle, and interfacial water structure, Chem, 8 (2022) 1187-1200.

[103] A. Mabudi, M. Noaparast, M. Gharabaghi, V.R. Vasquez, A molecular dynamics study on the wettability of graphene-based silicon dioxide (glass) surface, Colloids and Surfaces A: Physicochemical and Engineering Aspects, 569 (2019) 43-51.

[104] L. Cui, X. Chen, B. Liu, K. Chen, Z. Chen, Y. Qi, H. Xie, F. Zhou, M.H. Rummeli, Y. Zhang, Z. Liu, Highly Conductive Nitrogen-Doped Graphene Grown on Glass toward Electrochromic Applications, ACS Appl Mater Interfaces, 10 (2018) 32622-32630.

[105] N. Wei, Q. Li, S. Cong, H. Ci, Y. Song, Q. Yang, C. Lu, C. Li, G. Zou, J. Sun, Y. Zhang, Z. Liu, Direct synthesis of flexible graphene glass with macroscopic uniformity enabled by copper-foam-assisted PECVD, Journal of Materials Chemistry A, 7 (2019) 4813-4822.

[106] A. Ashraf, Y. Wu, M.C. Wang, K. Yong, T. Sun, Y. Jing, R.T. Haasch, N.R. Aluru, S. Nam, Doping-Induced Tunable Wettability and Adhesion of Graphene, Nano Lett, 16 (2016) 4708-4712.

[107] T. Tian, S. Lin, S. Li, L. Zhao, E.J.G. Santos, C.J. Shih, Doping-Driven Wettability of Two-Dimensional Materials: A Multiscale Theory, Langmuir, 33 (2017) 12827-12837.

[108] G. Giovannetti, P.A. Khomyakov, G. Brocks, V.M. Karpan, J. van den Brink, P.J. Kelly, Doping graphene with metal contacts, Phys Rev Lett, 101 (2008) 026803.

[109] G. Hong, Y. Han, T.M. Schutzius, Y. Wang, Y. Pan, M. Hu, J. Jie, C.S. Sharma, U. Muller, D. Poulikakos, On the Mechanism of Hydrophilicity of Graphene, Nano Lett, 16 (2016) 4447-4453.

[110] X. Tan, Z. Zhou, M.M. Cheng, Electrowetting on dielectric experiments using graphene, Nanotechnology, 23 (2012) 375501.

[111] A. Shahini, J. Xia, Z. Zhou, Y. Zhao, M.M. Cheng, Versatile Miniature Tunable Liquid Lenses Using Transparent Graphene Electrodes, Langmuir, 32 (2016) 1658-1665.

[112] J. Park, H.-K. Park, J. Choi, Scalable Graphene Electro-Patterning, Functionalization, and Printing, The Journal of Physical Chemistry C, 121 (2017) 14954-14961.

[113] Z. Zhai, H. Shen, J. Chen, X. Li, Y. Li, Metal-Free Synthesis of Boron-Doped Graphene Glass by Hot-Filament Chemical Vapor Deposition for Wave Energy Harvesting, ACS Appl Mater Interfaces, 12 (2020) 2805-2815.

[114] H. Choi, H.-H. Jo, S. Hwang, M. Jeon, J.-H. Kim, Synthesis of sulfur-doped graphene by using Near-infrared chemical-vapor deposition, Journal of the Korean Physical Society, 68 (2016) 1257-1261.

[115] S.T. Pantelides, Y. Puzyrev, L. Tsetseris, B. Wang, Defects and doping and their role in functionalizing graphene, MRS Bulletin, 37 (2012) 1187-1194.

[116] Z. Hu, Y. Zhao, W. Zou, Q. Lu, J. Liao, F. Li, M. Shang, L. Lin, Z. Liu, Doping of Graphene Films: Open the way to Applications in Electronics and Optoelectronics, Advanced Functional Materials, 32 (2022).

[117] N. Liu, J. Zhang, Y. Chen, C. Liu, X. Zhang, K. Xu, J. Wen, Z. Luo, S. Chen, P. Gao, K. Jia, Z. Liu, H. Peng, H.W. Wang, Bioactive Functionalized Monolayer Graphene for High-Resolution Cryo-Electron Microscopy, J Am Chem Soc, 141 (2019) 4016-4025.

[118] M. Dieng, M. Bensifia, J. Borme, I. Florea, C.M. Abreu, C. Jama, C. Léonard, P. Alpuim, D. Pribat, A. Yassar, F.Z. Bouanis, Wet-Chemical Noncovalent Functionalization of CVD Graphene: Molecular Doping and Its Effect on Electrolyte-Gated Graphene Field-Effect Transistor Characteristics, The Journal of Physical Chemistry C, 126 (2022) 4522-4533.

[119] Y. Taniguchi, T. Miki, T. Mitsuno, Y. Ohno, M. Nagase, K. Minagawa, M. Yasuzawa, Fabrication of hydrophilic graphene film by molecular functionalization, physica status solidi (b), 254 (2017).

[120] X.V. Zhen, E.G. Swanson, J.T. Nelson, Y. Zhang, Q. Su, S.J. Koester, P. Bühlmann, Noncovalent Monolayer Modification of Graphene Using Pyrene and Cyclodextrin Receptors for Chemical Sensing, ACS Applied Nano Materials, 1 (2018) 2718-2726.

[121] T. Okada, G. Kalita, M. Tanemura, I. Yamashita, M. Meyyappan, S. Samukawa, Nitrogen doping effect on flow-induced voltage generation from graphene-water interface, Applied Physics Letters, 112 (2018).

[122] Y. Xia, Y. Sun, H. Li, S. Chen, T. Zhu, G. Wang, B. Man, J. Pan, C. Yang, Plasma treated graphene FET sensor for the DNA hybridization detection, Talanta, 223 (2021) 121766.

[123] L. Zheng, N. Liu, Y. Liu, N. Li, J. Zhang, C. Wang, W. Zhu, Y. Chen, D. Ying, J. Xu, Z. Yang, X. Gao, J. Tang, X. Wang, Z. Liang, R. Zou, Y. Li, P. Gao, X. Wei, H.W. Wang, H. Peng, Atomically Thin Bilayer Janus Membranes for Cryo-electron Microscopy, ACS Nano, 15 (2021) 16562-16571.

[124] L. Zheng, N. Liu, X. Gao, W. Zhu, K. Liu, C. Wu, R. Yan, J. Zhang, X. Gao, Y. Yao, B. Deng, J. Xu, Y. Lu, Z. Liu, M. Li, X. Wei, H.W. Wang, H. Peng, Uniform thin ice on ultraflat graphene for high-resolution cryo-EM, Nat Methods, 20 (2023) 123-130.

[125] J. Son, J.Y. Lee, N. Han, J. Cha, J. Choi, J. Kwon, S. Nam, K.H. Yoo, G.H. Lee, J. Hong, Tunable Wettability of Graphene through Nondestructive Hydrogenation and Wettability-Based Patterning for Bioapplications, Nano Lett, 20 (2020) 5625-5631.

[126] J. Seo, W.S. Chang, T.-S. Kim, Adhesion improvement of graphene/copper interface using UV/ozone treatments, Thin Solid Films, 584 (2015) 170-175.

[127] H. Sun, D. Chen, Y. Wu, Q. Yuan, L. Guo, D. Dai, Y. Xu, P. Zhao, N. Jiang, C.-T. Lin, High quality graphene films with a clean surface prepared by an UV/ozone assisted transfer process, Journal of Materials Chemistry C, 5 (2017) 1880-1884.

[128] K.C. Kwon, W.J. Dong, G.H. Jung, J. Ham, J.-L. Lee, S.Y. Kim, Extension of stability in organic photovoltaic cells using UV/ozone-treated graphene sheets, Solar Energy Materials and Solar Cells, 109 (2013) 148-154.

[129] A.H. Alami, K. Aokal, A.G. Olabi, S. Alasad, H. Aljaghoub, Applications of graphene for energy harvesting applications: Focus on mechanical synthesis routes for graphene production, Energy Sources, Part A: Recovery, Utilization, and Environmental Effects, (2021) 1-30.

[130] F. Bonaccorso, L. Colombo, G. Yu, M. Stoller, V. Tozzini, A.C. Ferrari, R.S. Ruoff, V. Pellegrini, 2D materials. Graphene, related two-dimensional crystals, and hybrid systems for energy conversion and storage, Science, 347 (2015) 1246501.

[131] Y.H. Hu, H. Wang, B. Hu, Thinnest two-dimensional nanomaterial-graphene for solar energy, ChemSusChem, 3 (2010) 782-796.

[132] J. Zhu, D. Yang, Z. Yin, Q. Yan, H. Zhang, Graphene and graphene-based materials for energy storage applications, Small, 10 (2014) 3480-3498.

[133] K. Jia, J. Zhang, Y. Zhu, L. Sun, L. Lin, Z. Liu, Toward the commercialization of chemical vapor deposition graphene films, Applied Physics Reviews, 8 (2021) 041306.

[134] H. Su, T. Wu, D. Cui, X. Lin, X. Luo, Y. Wang, L. Han, The Application of Graphene Derivatives in Perovskite Solar Cells, Small Methods, 4 (2020).

[135] P. You, G. Tang, F. Yan, Two-dimensional materials in perovskite solar cells, Materials Today Energy, 11 (2019) 128-158.

[136] A. Suhail, G. Pan, D. Jenkins, K. Islam, Improved efficiency of graphene/Si Schottky junction solar cell based on back contact structure and DUV treatment, Carbon, 129 (2018) 520-526.

[137] M.A. Rehman, I. Akhtar, W. Choi, K. Akbar, A. Farooq, S. Hussain, M.A. Shehzad, S.-H. Chun, J. Jung, Y. Seo, Influence of an Al2O3 interlayer in a directly grown graphene-silicon Schottky junction solar cell, Carbon, 132 (2018) 157-164.

[138] H.A. Busaidi, A. Suhail, D. Jenkins, G. Pan, Developed graphene/Si Schottky junction solar cells based on the top-window structure, Carbon Trends, 10 (2023).

[139] J. Zhang, J. Fan, B. Cheng, J. Yu, W. Ho, Graphene - Based Materials in Planar Perovskite Solar Cells, Solar RRL, 4 (2020).

[140] G. Jeong, D. Koo, J. Seo, S. Jung, Y. Choi, J. Lee, H. Park, Suppressed Interdiffusion and Degradation in Flexible and Transparent Metal Electrode-Based Perovskite Solar Cells with a Graphene Interlayer, Nano Lett, 20 (2020) 3718-3727.

[141] S. Lee, J.S. Yeo, Y. Ji, C. Cho, D.Y. Kim, S.I. Na, B.H. Lee, T. Lee, Flexible organic solar cells composed of P3HT:PCBM using chemically doped graphene electrodes, Nanotechnology, 23 (2012) 344013.

[142] Y. Lin, X. Li, D. Xie, T. Feng, Y. Chen, R. Song, H. Tian, T. Ren, M. Zhong, K. Wang, Graphene/semiconductor heterojunction solar cells with modulated antireflection and graphene work function, Energy & environmental science, 6 (2013) 108-115.

[143] Z. Yin, J. Zhu, Q. He, X. Cao, C. Tan, H. Chen, Q. Yan, H. Zhang, Graphene-Based Materials for Solar Cell Applications, Advanced Energy Materials, 4 (2014).

[144] S. Das, P. Sudhagar, Y.S. Kang, W. Choi, Graphene synthesis and application for solar cells, Journal of Materials Research, 29 (2014) 299-319.

[145] Y. Xia, Y. Pan, H. Zhang, J. Qiu, Y. Zheng, Y. Chen, W. Huang, Graphene Oxide by UV-Ozone Treatment as an Efficient Hole Extraction Layer for Highly Efficient and Stable Polymer Solar Cells, ACS Appl Mater Interfaces, 9 (2017) 26252-26256.

[146] S. Yavuz, E.M. Loran, N. Sarkar, D.P. Fenning, P.R. Bandaru, Enhanced Environmental Stability Coupled with a 12.5% Power Conversion Efficiency in an Aluminum Oxide-Encapsulated n-Graphene/p-Silicon Solar Cell, ACS Appl Mater Interfaces, 10 (2018) 37181-37187.

[147] C. Lian, X. Kong, H. Liu, J. Wu, On the hydrophilicity of electrodes for capacitive energy extraction, J Phys Condens Matter, 28 (2016) 464008.

[148] H. Li, Y. Wen, M. Jiang, Y. Yao, H. Zhou, Z. Huang, J. Li, S. Jiao, Y. Kuang, S. Luo, Understanding of neighboring fe - n4 - c and co - n4 - c dual active centers for oxygen reduction reaction, Advanced Functional Materials, 31 (2021) 2011289.

[149] X. Zhang, J. Li, H. Ao, D. Liu, L. Shi, C. Wang, Y. Zhu, Y. Qian, Appropriately hydrophilic/hydrophobic cathode enables high-performance aqueous zinc-ion batteries, Energy Storage Materials, 30 (2020) 337-345.

[150] S. Li, Y. Liu, X. Zhao, Q. Shen, W. Zhao, Q. Tan, N. Zhang, P. Li, L. Jiao, X. Qu, Sandwich-Like Heterostructures of MoS(2) /Graphene with Enlarged Interlayer Spacing and Enhanced Hydrophilicity as High-Performance Cathodes for Aqueous Zinc-Ion Batteries, Adv Mater, 33 (2021) e2007480.

[151] H. Zhang, R. Guo, S. Li, C. Liu, H. Li, G. Zou, J. Hu, H. Hou, X. Ji, Graphene quantum dots enable dendrite-free zinc ion battery, Nano Energy, 92 (2022).

[152] X. Yang, X. Zheng, H. Li, B. Luo, Y. He, Y. Yao, H. Zhou, Z. Yan, Y. Kuang, Z. Huang, Non - Noble - Metal Catalyst and Zn/Graphene Film for Low - Cost and Ultra - Long - Durability Solid - State Zn - Air Batteries in Harsh Electrolytes, Advanced Functional Materials, 32 (2022) 2200397.

[153] J. Sun, B. Luo, H. Li, A Review on the conventional capacitors, supercapacitors, and emerging hybrid ion capacitors: Past, present, and future, Advanced Energy and Sustainability Research, 3 (2022) 2100191.

[154] J. Tian, S. Wu, X. Yin, W. Wu, Novel preparation of hydrophilic graphene/graphene oxide nanosheets for supercapacitor electrode, Applied Surface Science, 496 (2019).

[155] E. Uesugi, H. Goto, R. Eguchi, A. Fujiwara, Y. Kubozono, Electric double-layer capacitance between an ionic liquid and few-layer graphene, Sci Rep, 3 (2013) 1595.

[156] S.S. Kwon, J. Choi, M. Heiranian, Y. Kim, W.J. Chang, P.M. Knapp, M.C. Wang, J.M. Kim, N.R. Aluru, W.I. Park, S. Nam, Electrical Double Layer of Supported Atomically Thin Materials, Nano Lett, 19 (2019) 4588-4593.

[157] P. Dhiman, F. Yavari, X. Mi, H. Gullapalli, Y. Shi, P.M. Ajayan, N. Koratkar, Harvesting energy from water flow over graphene, Nano Lett, 11 (2011) 3123-3127.

[158] J. Yin, Z. Zhang, X. Li, J. Zhou, W. Guo, Harvesting energy from water flow over graphene?, Nano Lett, 12 (2012) 1736-1741.

[159] J. Yin, Z. Zhang, X. Li, J. Yu, J. Zhou, Y. Chen, W. Guo, Waving potential in graphene, Nat Commun, 5 (2014) 3582.

[160] W. Fei, C. Shen, S. Zhang, H. Chen, L. Li, W. Guo, Waving potential at volt level by a pair of graphene sheets, Nano Energy, 60 (2019) 656-660.

[161] Y. Yan, X. Zhou, S. Feng, Y. Lu, J. Qian, P. Zhang, X. Yu, Y. Zheng, F. Wang, K. Liu, S. Lin, Direct Current Electricity Generation from Dynamic Polarized Water–Semiconductor Interface, The Journal of Physical Chemistry C, 125 (2021) 14180-14187.

[162] H. Cai, Y. Guo, W. Guo, Synergistic effect of substrate and ion-containing water in graphene based hydrovoltaic generators, Nano Energy, 84 (2021).

[163] J. Shan, S. Fang, W. Wang, W. Zhao, R. Zhang, B. Liu, L. Lin, B. Jiang, H. Ci, R. Liu, W. Wang, X. Yang, W. Guo, M.H. Rummeli, W. Guo, J. Sun, Z. Liu, Copper acetate-facilitated transfer-free growth of high-quality graphene for hydrovoltaic generators, Natl Sci Rev, 9 (2022) nwab169.

[164] S.S. Kwak, S. Lin, J.H. Lee, H. Ryu, T.Y. Kim, H. Zhong, H. Chen, S.W. Kim, Triboelectrification-Induced Large Electric Power Generation from a Single Moving Droplet on Graphene/Polytetrafluoroethylene, ACS Nano, 10 (2016) 7297-7302.

[165] M.A.H. Mudhafar, H.-Y. Pan, Optimization of Condensation Heat Transfer on enhanced and integral fin tubes by Functionalized-Graphene Layers, Heat and Mass Transfer, 58 (2022) 2147-2160.

[166] W. Chang, B. Peng, K. Egab, Y. Zhang, Y. Cheng, X. Li, X. Ma, C. Li, Few-layer graphene on nickel enabled sustainable dropwise condensation, Sci Bull (Beijing), 66 (2021) 1877-1884.

[167] J.Y. Kim, K.M. Kim, I.C. Bang, Effect of 2-D Plane Graphene Thermal Effusivity on Boiling Heat Transfer with Highly Wettable FC-72, Transactions of the Korean Nuclear Society Autumn Meeting Goyang, Korea, , 2019.

[168] J. Pei, Y. Liao, Q. Li, K. Shi, J. Fu, X. Hu, Z. Huang, L. Xue, X. Xiao, K. Liu, Single-layer graphene prevents Cassie-wetting failure of structured hydrophobic surface for efficient condensation, J Colloid Interface Sci, 615 (2022) 302-308.

[169] L. Tan, M. Zeng, Q. Wu, L. Chen, J. Wang, T. Zhang, J. Eckert, M.H. Rummeli, L. Fu, Direct growth of ultrafast transparent single-layer graphene defoggers, Small, 11 (2015) 1840-1846.

[170] Z. Wang, Z. Xue, M. Zhang, Y. Wang, X. Xie, P.K. Chu, P. Zhou, Z. Di, X. Wang, Germanium-Assisted Direct Growth of Graphene on Arbitrary Dielectric Substrates for Heating Devices, Small, 13 (2017).

[171] Z. Chen, Y. Qi, X. Chen, Y. Zhang, Z. Liu, Direct CVD Growth of Graphene on Traditional Glass: Methods and Mechanisms, Adv Mater, 31 (2019) e1803639.

[172] A. Khan, S.M. Islam, S. Ahmed, R.R. Kumar, M.R. Habib, K. Huang, M. Hu, X. Yu, D. Yang, Direct CVD Growth of Graphene on Technologically Important Dielectric and Semiconducting Substrates, Adv Sci (Weinh), 5 (2018) 1800050.

[173] S. Wu, G. Xiong, H. Yang, B. Gong, Y. Tian, C. Xu, Y. Wang, T. Fisher, J. Yan, K. Cen, T. Luo, X. Tu, Z. Bo, K. Ostrikov, Multifunctional Solar Waterways: Plasma - Enabled Self - Cleaning Nanoarchitectures for Energy - Efficient Desalination, Advanced Energy Materials, 9 (2019).

[174] D. Kim, E. Kim, S. Park, S. Kim, B.K. Min, H.J. Yoon, K. Kwak, M. Cho, Wettability of graphene and interfacial water structure, Chem, 7 (2021) 1602-1614.

[175] C.H. Lin, M.S. Tsai, W.T. Chen, Y.Z. Hong, P.Y. Chien, C.H. Huang, W.Y. Woon, C.T. Lin, A low-damage plasma surface modification method of stacked graphene bilayers for configurable wettability and electrical properties, Nanotechnology, 30 (2019) 245709.

[176] H. Zhong, J. Xia, F. Wang, H. Chen, H. Wu, S. Lin, Graphene-Piezoelectric Material Heterostructure for Harvesting Energy from Water Flow, Advanced Functional Materials, 27 (2017).